AGU PUBLICATIONS

JGR

Journal of Geophysical Research: Atmospheres

RESEARCH ARTICLE
10.1002/2014JD021983

Key Points:
- Interannual to multidecadal blocking variability is decomposed in patterns
- Blocking patterns have a specific impact on extreme temperatures
- Blocking variability patterns are related to the NAO, AMO, and solar forcing

Supporting Information:
- Readme
- Figure S1
- Figure S2
- Figure S3
- Figure S4
- Figure S5
- Figure S6
- Figure S7

Correspondence to:
N. Rimbu,
Norel.Rimbu@awi.de

Citation:
Rimbu, N., G. Lohmann, and M. Ionita (2014), Interannual to multidecadal Euro-Atlantic blocking variability during winter and its relationship with extreme low temperatures in Europe, *J. Geophys. Res. Atmos.*, *119*, 13,621–13,636, doi:10.1002/2014JD021983.

Received 16 MAY 2014
Accepted 16 NOV 2014
Accepted article online 25 NOV 2014
Published online 16 DEC 2014

Interannual to multidecadal Euro-Atlantic blocking variability during winter and its relationship with extreme low temperatures in Europe

Norel Rimbu[1,2,3], Gerrit Lohmann[1,4], and Monica Ionita[1,4]

[1]Alfred Wegener Institute Helmholtz Centre for Polar and Marine Research, Bremerhaven, Germany, [2]University of Bucharest, Faculty of Physics, Bucharest, Romania, [3]Climed Norad, Bucharest, Romania, [4]MARUM—Center for Marine Environmental Sciences, University of Bremen, Bremen, Germany

Abstract The dominant modes of blocking frequency variability in the Atlantic-European region are evaluated for the 1871–2010 period. An Empirical Orthogonal Function (EOF) analysis of a two-dimensional blocking indicator field reveals three dominant EOFs, describing about 35% of interannual to multidecadal blocking variability. The first EOF captures an out-of-phase blocking frequency anomaly over Greenland and Western Europe regions. The corresponding principal component time series is strongly correlated with the North Atlantic Oscillation index but shows also significant correlations with indices of the East Atlantic, Scandinavian, and East Atlantic-Western Russia patterns. The second EOF shows a dominant center over the North Sea region as well as a less pronounced center with anomalies of the same sign over southeastern Greenland. The multidecadal variations of this mode of blocking variability are related with a basin wide North Atlantic sea surface temperature anomaly which projects partly on the Atlantic Multidecadal Oscillation (AMO). The third mode is an east-west dipole of blocking frequency anomalies from Scandinavian and southern Greenland regions and shows enhanced variability at ~20 year time scales. The coherent variations of the time coefficients of this pattern with open solar flux suggest a possible solar influence on blocking variability at these time scales. Furthermore, the dominant patterns of blocking variability are related with distinct anomaly patterns in the occurrence of extreme low temperature events over Europe at interannual to multidecadal time scales. AMO as well as the solar signals was detected also in the corresponding extreme low temperature blocking patterns. We argue that multivariate analysis of blocking indicators gives additional information about blocking and related extreme climate phenomena variability and predictability comparative with classical sectorial approach.

1. Introduction

Atmospheric blocking is a large-scale midlatitude atmospheric phenomenon often associated with a split in the zonal jet as well as with persistent quasi-stationary synoptic-scale high pressure systems [e.g., *Diao et al.,* 2006]. It causes large-scale circulation anomalies exerting a strong impact upon the weather patterns and therefore is associated with significant climate anomalies [*Silmann and Croci-Maspoli*, 2009; *Silmann et al.*, 2011; *Pfahl and Wernli,* 2012].

Many studies have derived a comprehensive set of climatological statistical characteristics of blocking events using subjective or objective techniques, including location, frequency, duration, intensity, size, and distribution [e.g., *Barriopedro et al.,* 2010]. In the Northern Hemisphere blocking occurs over the whole extratropical region. Preferred Northern Hemisphere locations for blocking are the end of the Pacific and Atlantic jet streams [e.g., *Cheung et al.,* 2013]. Relatively high frequency of blocking events is also recorded in the Ural Mountains region (near 60°E) and north-eastern part of Canada [e.g., *Diao et al.,* 2006].

Many studies [*Barriopedro et al.,* 2006; *Davini et al.,* 2012; *Barnes et al.,* 2014*; Cheung et al.*, 2013] investigate possible linear trends in the Northern Hemisphere blocking frequency or intensity. These linear trends are usually estimated within several subjectively chosen sectors of the Northern Hemisphere, such as the Atlantic (ATL), European (EUR), West Pacific (WPA), and East Pacific (EPA) sectors [*Barriopedro et al.,* 2006]. Significant negative (positive) linear trends in annual blocking frequency over EUR and ATL (WPA) sectors during 1948–2002 were identified [*Barriopedro et al.,* 2006]. *Cheung et al.* [2013] show that winter blocking exhibits decreasing frequency over the whole Northern Hemisphere but not significant trends over several

sectors of Asia-Pacific region over the period 1950–2009. More recently, *Barnes et al.* [2014] investigate the blocking frequency trends during last decades (1980/1995–2012) using various blocking indices and four different reanalysis. They find robust seasonal increases and decreases for some isolated regions, but not for the entire Northern Hemisphere. *Davini et al.* [2012] show a complex spatial pattern of winter blocking frequency linear trends over the Northern Hemisphere during the period 1951–2010 with a marked increase of low-latitude blocking over the Atlantic, a general reduction of blocking over Siberia, and a dipole pattern over Greenland. More general, the frequency of high-latitude blocking during 1951–2010 period show a decreasing trend [*Davini et al.,* 2012]. Model simulations [*de Vries et al.,* 2013a*; Dunn-Sigouin and Son,* 2013] show also complex blocking patterns in the Atlantic realm in future climate during winter. Particularly, in the SRES A1b emission scenario beyond the year 2000 a clear reduction of blocking frequency over the Atlantic and an increase over central and northeastern Europe as well as at higher latitudes were detected [*de Vries et al.,* 2013a].

Superimposed on the linear trends, the blocking frequency shows important interannual and decadal variability [*Barriopedro et al.*, 2006; *Rimbu and Lohmann,* 2011; *Häkkinen et al.,* 2011; *Davini et al.,* 2012; *Barnes et al.,* 2014]. These variations are related to the interannual and decadal variability of the North Atlantic Oscillation (NAO) [*Shabbar et al.,* 2001], El Niño-Southern Oscillation (ENSO), and Pacific-North-American (PNA) pattern [*Croci-Maspoli et al.,* 2007] or Pacific Decadal Oscillation [*Chen and Yoon,* 2002]. Multidecadal variations of the blocking frequency in the North Atlantic were related to Atlantic Multidecadal Oscillation (AMO) [*Häkkinen et al.,* 2011].

The studies mentioned above reveal that blocking trends as well as interannual to multidecadal variability present complex spatial patterns over the Northern Hemisphere. As the two-dimensional (2-D) blocking indices are calculated both for observational and model data [*Scherrer et al.,* 2006; *Davini et al.,* 2012; *Masato et al.,* 2013] over relatively long periods, multivariate statistical methods can be used to identify patterns of blocking variability. Instead of using subjectively defined sectors to study blocking variability or to calculate blocking patterns associated to different climate modes [*Scherrer et al.*, 2006] we used here Empirical Orthogonal Functions (EOF) technique [e.g., *von Storch and Zwiers,* 1999] applied to a 2-D blocking indicator to identify the dominant spatial and temporal patterns of interannual to multidecadal blocking variability in the Euro-Atlantic region. The 2-D patterns of blocking variability identified with EOF technique could give additional information about spatial and temporal variability of blocking comparative with classical regional blocking indices. Therefore, the patterns of blocking variability, derived through EOF analysis, will be discussed in connection with classical sectorial blocking variability as described in previous studies.

Atmospheric blocking conditions not only influence the mean winter climate but also extreme temperature and precipitation events over the Euro-Atlantic region [*Silmann and Croci-Maspoli*, 2009; *Silmann et al.*, 2011; *Pfahl and Wernli,* 2012]. Persistent atmospheric blocking conditions in the North Atlantic realm disturb the predominant westerly flow over Europe favoring a northeastern inflow of cold and dry air masses [*Trigo et al.,* 2004]. Persistent clear-sky conditions favor increased outgoing long wave radiation during winter nights and results in strong cooling of the earth surface and anomalous cold surface temperatures [*Trigo et al.,* 2004]. Blocking impacts also extreme precipitation events, drought, and other severe weather phenomena [e.g., *Andrade et al.,* 2012; *Pfahl and Wernli,* 2012]. The connection between blocking and extreme fields can be investigated also through multivariate methods like Canonical Correlation Analysis [e.g., *von Storch and Zwiers,* 1999]. For simplicity, in our study we used simple linear correlation analysis to establish the low extreme temperature patterns associated to the dominant patterns of blocking variability in the North Atlantic region.

The main goal of this study is to identify the dominant patterns of the Euro-Atlantic interannual to multidecadal variability of the blocking frequency during winter as well as their associated patterns in the field of the frequency of extremely low temperature events in Europe.

The paper is organized as follows. Data and methods are presented in section 2. The dominant spatial and temporal patterns of interannual to multidecadal variability in the blocking frequency over the Atlantic-European region and their relationships with relevant atmospheric teleconnection patterns are presented in section 3. The relationship between the dominant patterns of blocking variability and extreme low temperature over Europe is presented in section 4. A discussion and the main conclusions follow in section 5.

2. Data and Methods

The data used in this study to calculate the blocking frequency are the winter daily 500 mb geopotential height (Z500) extracted from the 20th Century Reanalysis Project database (20CR) (available at http://www.esrl.noaa.gov/psd/data/gridded/data.20thC-ReanV2.html), version 2, for the period 1871–2010. This reanalysis incorporates observations of sea level pressure and surface pressure alone [*Compo et al.,* 2011]. Observed sea surface temperature (SST) and sea-ice concentration data are used as boundary conditions. The reanalysis used the coupled atmosphere-land version of the NOAA NCEP global forecast model run with 56 ensemble members, which allows an estimate of errors function of data availability. We used the daily ensemble mean Z500 field on a regular longitude-latitude grid of $2° \times 2°$ resolution covering the Northern Hemisphere (20°N–90°N) to calculate blocking frequency. The key feature of the use of 20CR in our study is the unprecedented length of the data which allow us to investigate blocking variability at interannual to multidecadal time scales.

We interpolate linearly the Z500 field on a 2.5° latitude × 2.5° longitude grid to facilitate a comparison with the blocking frequency based on NCEP/NCAR reanalysis (hereafter NCEP1) data [*Kalnay et al.,* 1996], widely used to calculate blocking frequency starting with 1948. The blocking frequency is based on 12,510 maps of the Northern Hemisphere (poleward to 20°N) daily Z500 field. We have used also the Z500 daily fields from NCEP1 [*Kalnay et al.,* 1996] for the period 1948–2010 as well as from ERA-40 [*Uppala et al.,* 2005] (available at http://www.ecmwf.int/products/data/arcchive/) for the period 1958–2001. The blocking patterns based on NCEP1 and ERA-40 data are compared with the corresponding blocking patterns obtained using the 20CR data.

As a measure of blocking frequency we have used the 2-D index described by *Scherrer et al.* [2006]. It is an extension of the one-dimensional (1-D) Tibaldi-Molteni (TM) index [*Tibaldi and Molteni,* 1990] to a two-dimensional map of blocking frequencies at every grid point. For each grid point the southern gradient (GHGS) and the northern gradient (GHGN) are evaluated as follows:

$$GHGS = (Z(\varphi_0) - Z(\varphi_0 - 15°))/15°$$
$$GHGN = (Z(\varphi_0 + 15°) - Z(\varphi_0))/15°$$

where φ_0 is the latitude of the considered grid point varying from 35°N to 75°N.

For each winter we calculate the ratio between the number of days when a certain grid point was blocked and the total number of winter days (90 days). A grid point is blocked if the conditions $GHGN > 0$ and $GHGS < (-10m/\circ.lat)$ are simultaneously satisfied for at least five consecutive days. We obtained 139 maps of frequency of blocked grid points, one per winter for the 1871–2010 period. These maps are referred here as blocking frequency (BF) field. The blocking frequency, calculated without any persistence criteria imposed, is referred in previous studies as instantaneous blocking frequency [e.g., *Davini et al.,* 2012]. Because we have used Z500 data for 20°N–90°N the BF field extends from 35°N to 75°N. We have to mention that this index, which is based on the reversal of the meridional gradient of Z500, does not provide any information about the spatial extension of the phenomena that is one of the main constraints to define a blocking event.

In order to compute the patterns of blocking variability, first, the linear trend of the BF field over the period 1871–2010 was removed. Then the BF anomalies relative to the mean over the period 1871–2010 were calculated. The dominant patterns of winter BF anomalies are identified using EOF analysis [*von Storch and Zwiers,* 1999]. EOFs were derived from covariance matrix of blocking anomalies.

Based on the same data set we calculate also the 1-D TM index [*Tibaldi and Molteni,* 1990] using the 55°N, 60°N, and 65°N reference latitudes and a 20° latitudinal interval to calculate the Z500 gradients. Through a composite analysis, we establish the 1-D blocking pattern associated to the positive and negative phases of the corresponding 2-D blocking pattern. Based on these composite maps we choose longitudinal sectors where the difference of 1-D blocking frequency of these composites is significantly different from zero and define regional blocking indices by imposing both temporal and spatial criteria. A certain sector is blocked if at least five consecutive longitudes, that is 12.5° longitude, are blocked for at least five consecutive days. These regional indices are compared with the time series of expansion coefficients (PCs) of the corresponding pattern of 2-D blocking variability.

The fields of the frequency of extremely low temperature events are calculated using the gridded data set E-OBS, version 8.0, for the period 1950 to 2010 [e.g., *van den Besselaar et al.,* 2011]. This data set has a

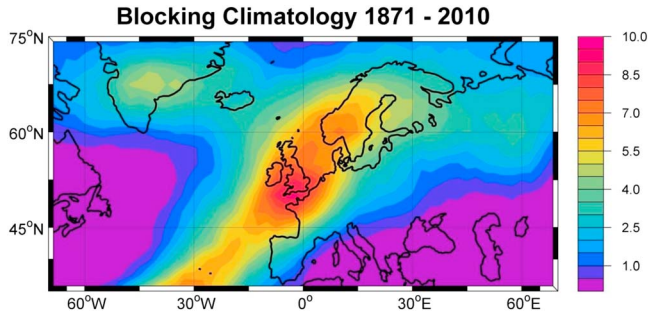

Figure 1. Winter blocking frequency climatology for the period 1871–2010. Units are percentage of blocked days to total number of days per season. Note that 1% blocking frequency corresponds to about one blocked day per season.

resolution of 0.5° latitude × 0.5° longitude and is based on long observational station data of the European Climate Assessment-Dataset (ECA&D) (available at http://www.ecad.eu). Extremely low temperature indices, referred to as the TN10p, are calculated for each grid point as the number of days in a winter when daily minimum temperature (TN) is lower than the 10th percentile. We use also station based TN10p indices, which are calculated based on long-term observational records from meteorological stations from Europe [*Klein Tank et al.,* 2002], and have been extracted also from the ECA&D data base. From a total of 4480 TN10p available records we selected 189 records distributed over Europe which cover the entire period 1900–2010 and have less than 20% of missing values.

Indices of the North Atlantic Oscillation (NAO), East Atlantic (EA), East Atlantic-Western Russia (EA-WR), and Scandinavian (SCA) teleconnection patterns over the period 1950–2010 have been obtained from the Climate Prediction Center (CPC) of the NOAA (available at www.cpc.ncep.noaa.gov). These indices were derived from a rotated principal component analysis applied to monthly mean standardized Z500 anomalies over 20°N–90°N. The time series of winter indices, derived through averaging the December, January, and February values, were correlated with the blocking pattern indices. The time series of the leading EOF of the winter (DJF) sea level pressure anomalies over the Atlantic sector, i.e., 20°N–80°N, 90°W–40°E, for the period 1899 to 2010, is also used as the NAO index in this study (available at https://climatedataguide.ucar.edu/climate-data/hurrell-north-atlantic-oscillation-nao-index-pc-based). The AMO index used in this study, which is basically an index of the North Atlantic temperatures, was downloaded from Earth System Research Laboratory (ESRL) (available at http://www.esrl.noaa.gov/psd/data/timeseries/AMO/), covering the period 1856 to present. The linear trend was removed from the AMO index prior to any analysis. The sea surface temperature (SST) over the North Atlantic region for the period 1871–2010 was extracted from the Extended Reconstructed Sea Surface Temperature data set [*Smith et al.,* 2008], version 3b (ERSST.v3b) (available at http://www.ncdc.noaa.gov). We have used also the time series of open solar flux (Fs), a measure of solar activity [*Lockwood et al.,* 2009], to find possible causes of decadal variability of blocking patterns. The Fs record, which covers the period 1675 to 2010 with annual resolution, was downloaded from http://climexp.knmi.nl/data/iosfa.txt.

Temporal periodic signals of blocking variability are identified using wavelet analysis [*Torrence and Compo,* 1998]. The analysis was performed using the software package from University of Colorado (http://paos.colorado.edu/research/wavelets/). Statistical significance is determined against a white noise null hypothesis using a chi-squared test. By decomposing a time series into a time-frequency space, it is possible to identify both stationary and non-stationary modes. The wavelet transform is designed to analyze time series that contain non-stationary power over different frequency scales [*Torrence and Compo,* 1998].

3. Patterns of Interannual to Multidecadal Blocking Variability

The blocking climatology is measured as the percentage of blocked days over the 139 winters for the 1871–2010 period. The 2-D blocking climatology map (Figure 1) shows two overlapping branches of relatively high blocking frequency similar to those presented in previous studies [*Scherrer et al.*, 2006; *Rimbu and Lohmann*, 2011; *Davini et al.,* 2012]. One branch extends west to east from the Labrador Sea to Scandinavia, while the other branch stretches from the Azores to southern Scandinavia. The maxima in the frequency of blocked grid points are located over southern Greenland, UK and Azores. A less pronounced blocking center is located at about 60°E, in the Ural Mountains region. Similar blocking climatology is obtained using NCEP1 (Figure S1b) as well as ERA-40 (Figure S1c) reanalysis data. However, over the common

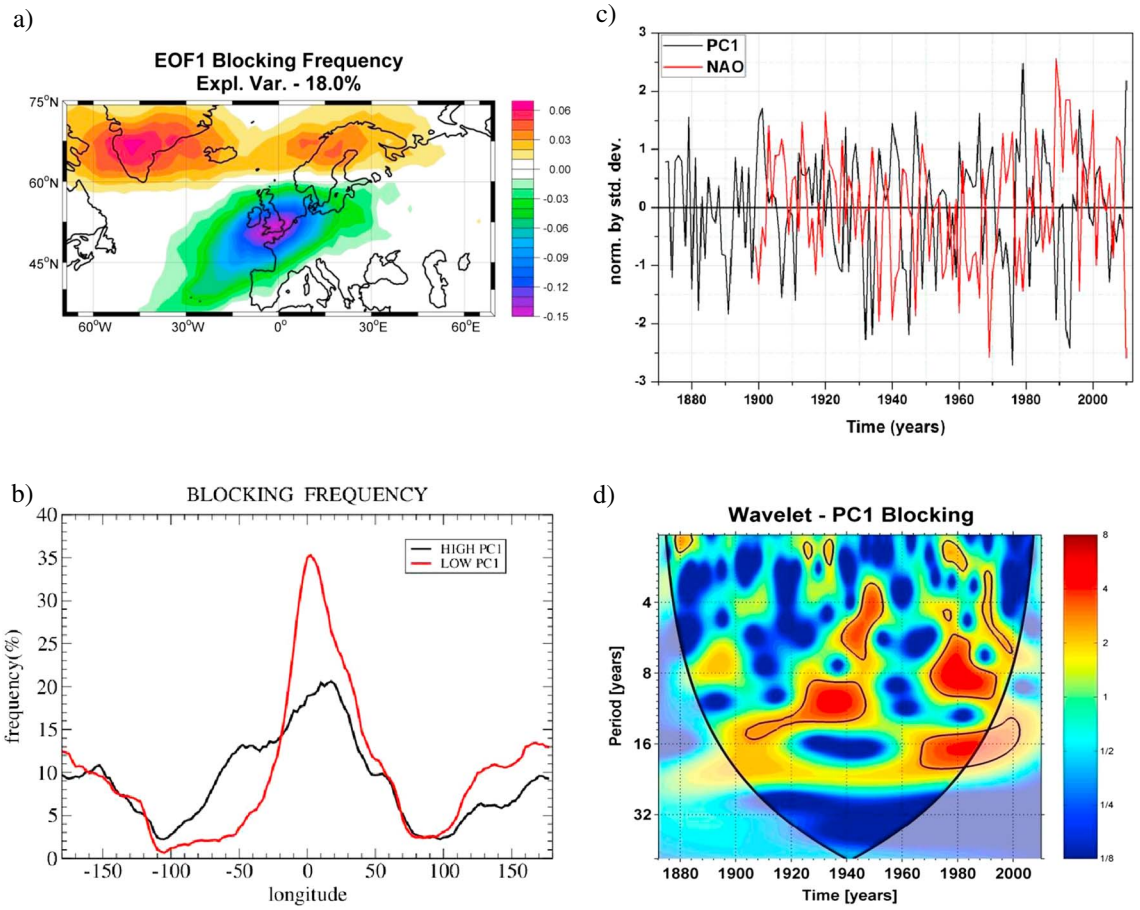

Figure 2. (a) The first Empirical Orthogonal Function (EOF) of blocking frequency variability; (b) blocking frequency associated to positive (black) and negative (red) phase of the pattern represented in Figure 2a as detected by one-dimensional Tibaldi-Molteni (TM) index; (c) the corresponding principal component (PC1) (black) and the North Atlantic Oscillation (NAO) index (red). (d) The continuous wavelet spectrum of PC1. The thick black contours designate the 90% significance level against white noise. The spectrum outside the cone of influence where the edge effects might be important is shown as a light shaded. Colors show power or variance.

period of reanalysis, the blocking frequency is higher in the North Sea region center for the 20CR (Figure S1a) relative to NCEP1 (Figure S1b) and ERA-40 (Figure S1c) data. The differences between blocking frequency in these reanalysis may arise from a number of reasons, like climatological biases or model horizontal or vertical resolution [e.g., *de Vries et al.,* 2013a]. Also by using of ensemble mean daily Z500 data from 20CR reanalysis to calculate the blocking frequency instead of ensemble members could influence the blocking frequency climatology. However, finding the exact reasons of such differences is beyond the scope of this study.

The patterns of blocking variability are calculated using blocking frequency anomalies relative to the climatology represented in Figure 1. The first three blocking patterns are discussed here because they are well separated according to North's rule [*North et al.,* 1982] and also have a physical interpretation.

The first EOF of BF anomalies (Figure 2a) describes 18% of the total variance. The positive phase of this pattern is associated with high blocking activity over the Greenland-Iceland and northern Scandinavia regions as well as with low blocking activity over a region centered over the northwestern part of Europe. This pattern of BF variability resembles the BF anomaly pattern associated to the negative phase of the NAO [*Scherrer et al.,* 2006]. Similar patterns are obtained using NCEP1 (Figure S2a) and ERA-40 (Figure S2b) blocking anomaly fields for the periods 1948–2010 and 1958–2001, respectively. Also the time coefficients (PC1) of NCEP1 and ERA-40 patterns are significantly positively correlated each other ($r = +0.58$) over the common periods (Figure S2c) and with PC1 of 20CR blocking pattern ($r = +0.90$ and $+0.55$, respectively).

A composite analysis reveals that positive (negative) phase of this blocking pattern is related to relative high (low) blocking frequency in 80°W–20°W (20°W–30°E) sector as detected with the 1-D TM index (Figure 2b).

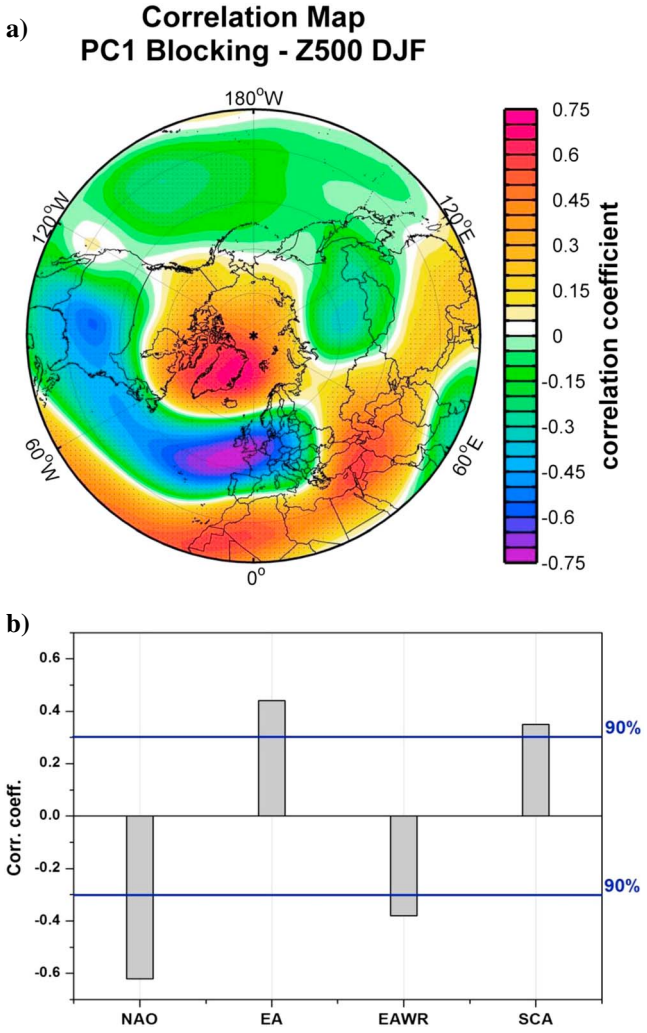

Figure 3. (a) Correlation map of winter blocking PC1 with Z500 for the period 1871–2010. The regions where correlation is above the 90% significance level are hatched; (b) the correlation coefficients between winter blocking PC1 and winter teleconnection indices for the period 1950–2010. Horizontal lines represent the 90% significance level.

Note the resemblance between blocking pattern represented in Figure 2b and the blocking pattern associated to the NAO [*Barriopedro et al.*, 2006; their Figure 9a]. The relatively low frequency of blocked longitudes in the (10°W–30°E) sector (Figure 2b) during positive phase of 2-D blocking pattern is related to low frequency of blocking over east Atlantic and western Europe (Figure 2a). The principal components time series (PC1) (Figure 2c) is significantly (90% level) negatively correlated ($r = -0.68$) with the NAO index for the period 1899–2010. The correlation increases ($r = -0.80$) if the PC1 and NAO time series are filtered in the decadal to multidecadal frequency band (time scales longer than 7 years). The wavelet spectrum of PC1 (Figure 2d), which is similar to the NAO wavelet spectrum [e.g., *Walter and Graf,* 2002], shows pronounced variability in the interannual and decadal band but does not show any stable periodic signal. The wavelet spectrum (Figure 2d) shows also relatively weak multidecadal variations of blocking PC1.

Based on the blocking frequency distribution represented in Figure 2b, we define two regional blocking indices as the number of days in a winter when the sectors (70°W–20°W) and (10°W–20°E) were blocked. A sector is blocked if at least five consecutive longitudes (12.5° longitude) within it are blocked for at least five consecutive days. The resulted blocking indices (not shown) are significantly (90% level) correlated ($r = +0.50$ and $r = -0.45$, respectively) with the blocking PC1. The difference of the normalized values of these blocking indices is significantly (90% level) positively correlated ($r = +0.66$) with blocking PC1. Therefore, the first pattern of the 2-D blocking variability (Figure 2a) reflects largely the out-of-phase blocking variability between the (70°W–20°W) and (10°W–20°E) sectors as captured by the 1-D TM index. Note the high values of both PC1 and blocking index during 2009/2010 winter when northern Europe was dominated by very low temperatures [*Cattiaux et al.*, 2010]. Anomalies of comparable magnitudes ($>1.5\sigma$) both in blocking PC1 and blocking index are recorded several times over the 1871–2010 period.

To understand the relationship between the first pattern of 2-D blocking variability and large-scale climate anomalies we constructed the correlation maps of blocking PC1 and Northern Hemisphere Z500 anomalies for the period 1871–2010. The correlation pattern (Figure 3a) contains elements of the NAO and EA-WR in their negative phases and of the EA and SCA in their positive phases. The pattern resembles the Z500 anomaly pattern that dominates the 2009/2010 winter [*Cattiaux et al.,* 2010], when several cold spells over northern and Western Europe were recorded. Note that the main negative Z500 anomaly centers of this pattern are located in the western and eastern part of the North Atlantic Ocean (Figure 3a). To better assess and confirm the relationship between the EOF1 of blocking variability and large-scale circulation, as shown

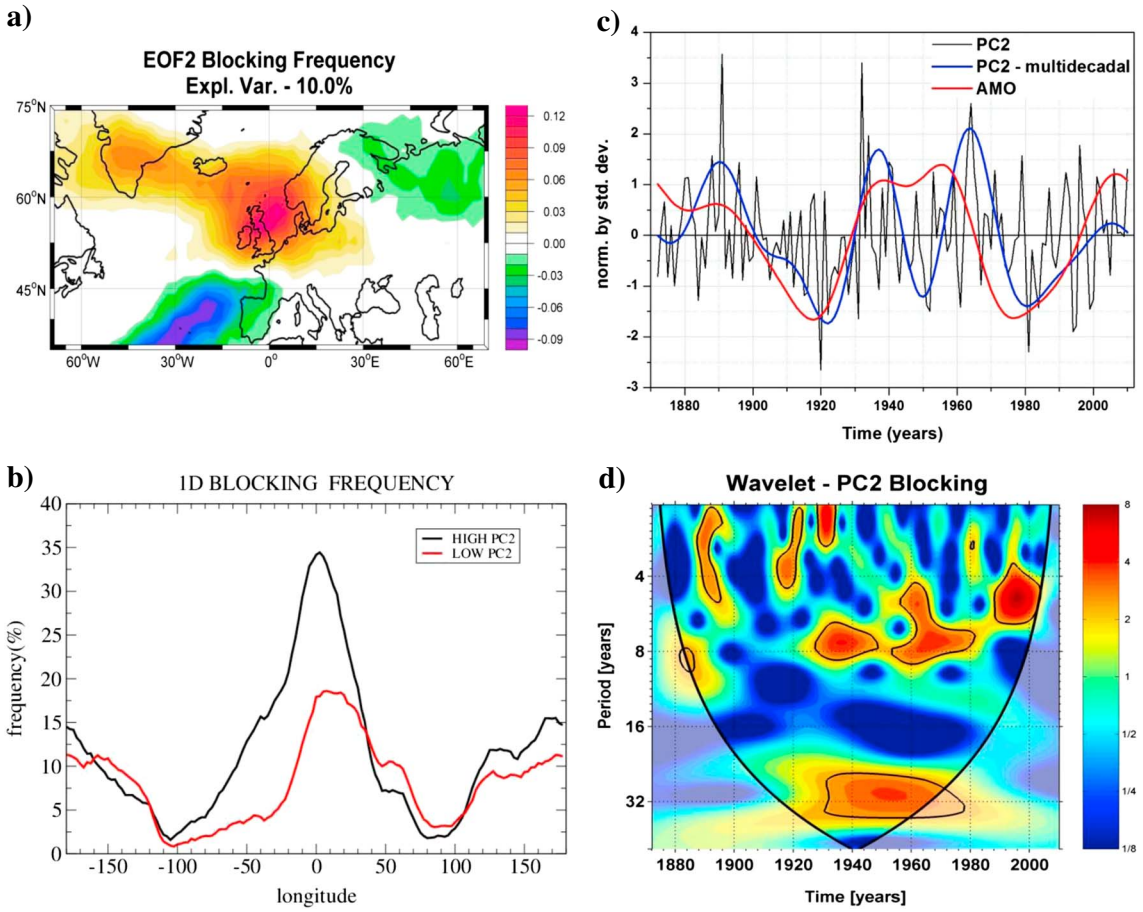

Figure 4. (a) The second EOF of blocking frequency variability; (b) blocking frequency associated to positive (black) and negative (red) phase of the pattern represented in (a) as detected by one-dimensional TM index; (c) the corresponding PC2 (black), its multidecadal (time scales longer than 20 years) component (blue) and the Atlantic Multidecadal Oscillation (AMO) index (red); (d) the wavelet continuous spectrum of PC2. The thick black contours designate the 90% significance level against white noise. The spectrum outside the cone of influence where the edge effects might be important is shown as a light shaded. Colors show power or variance.

by the correlation Z500 map (Figure 3a), we calculate the correlation coefficients between PC1 and the indices of the aforementioned teleconnection patterns for the period 1950–2010. Significant (90% level) positive correlations are obtained for the EA and the SCA indices, and significant negative correlations are obtained for the NAO and EA-WR indices, respectively (Figure 3b). The relationship of winter PC1 with different teleconnection patterns is not surprising, especially in light of the recent findings of *Comas-Bru and McDermott* [2013], which showed that the NAO centers are influenced by the phase of the SCA and EA patterns. According to the aforementioned study, when SCA and NAO are in opposite phases, the NAO dipole suffers a clockwise movement of its centers. A recent study [*Woollings and Blackburn*, 2012] shows that the NAO and EA patterns can be combined to describe the North Atlantic eddy-driven jet stream variability which is related with blocking variability. Blocking EOF1 (Figure 2a) shows pronounced loading centers over the Atlantic and Europe, where the blocking variability is modulated by different teleconnection patterns [e.g.,, *Scherrer et al.,* 2006; *Barriopedro et al.,* 2006]. This is consistent with the significant correlation between blocking PC1 and teleconnection pattern indices presented in Figure 3b.

The second EOF of BF variability, which describes 10% of the variance, shows a prominent center in the North Sea region as well as a less prominent center over the southeastern part of Greenland (Figure 4a). It resembles the blocking anomaly pattern associated to the third pattern of the winter Z500 variability from the Atlantic European region [*Scherrer et al.,* 2006; their Figure 8] which is closest the EA-WR teleconnection pattern. This pattern is similar to the EOF2 of blocking variability in NCEP1 (Figure S3a) and EOF3 of ERA-40 (Figure S3b). The corresponding time coefficients are significantly positively correlated ($r = +0.50$) over the common period (Figure S3c). The positive phase of this pattern is associated with

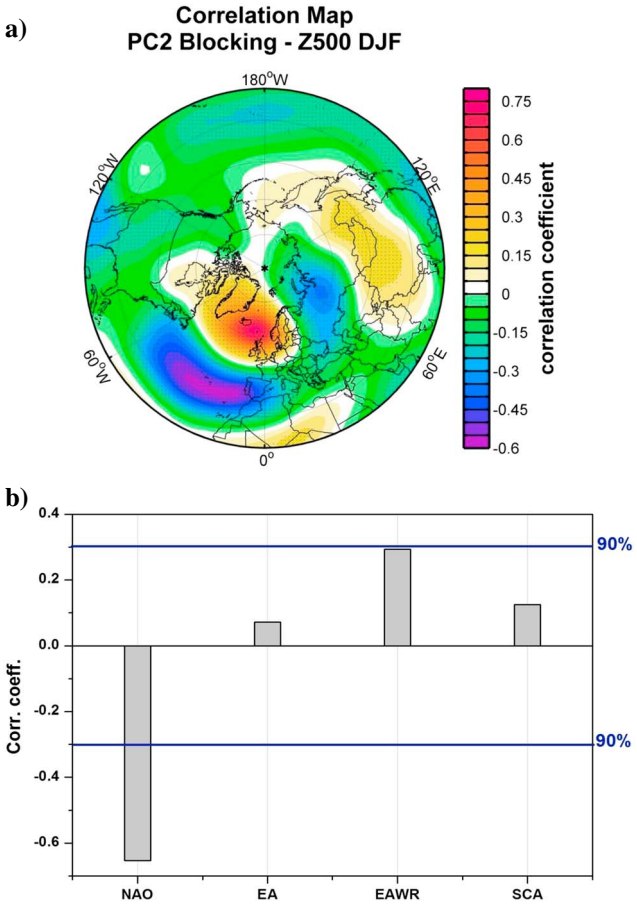

Figure 5. (a) Correlation map of winter blocking PC2 with Z500 for the period 1871–2010. The regions where correlation is above the 90% significance level are hatched; (b) the correlation coefficients between winter blocking PC2 and winter teleconnection indices for the period 1950–2010. Horizontal lines represent the 90% significance level.

relatively high blocking activity in the sector (80°W–40°E) as detected with classical TM blocking indicator (Figure 4b). The blocking PC2 is significantly positively correlated ($r = +0.83$) with the winter blocking frequency over the sector (80°W–20°E). Therefore, the second pattern of 2-D blocking variability (Figure 4a) largely reflects the blocking variability in the (80°W–20°E) as captured by regional 1-D TM index. Blocking PC2 (Figure 4c) shows pronounced decadal, but also multidecadal variations. Relatively high (low) frequency of blocking, as captured by this pattern, were recorded during winters of 1880–1900, 1930–1960, and 2000–2010 (1900–1930, 1970–1990) when the AMO was in its positive (negative) phase (Figure 4c, red thick line). Although the blocking frequency anomaly over the whole 1930–1960 is positive, the blocking PC2 shows relatively low values around 1950s, when a small decrease of the AMO index is recorded (Figure 4c). The wavelet spectrum of blocking PC2 (Figure 4d) shows several periodic but non stationary oscillations in the 4–8 year frequency interval as well as in the multidecadal band (Figure 4d). The ~30 year oscillation during 1920–1980 as detected in the wavelet spectrum (Figure 4d) reflects the multidecadal variability of blocking PC2 in this time interval (Figure 4c, thick blue line). Similar variations are detected also in the AMO index but with smaller amplitude (Figure 4c, red thick line).

The correlation map of PC2 and Z500 anomalies (Figure 5a) shows a wave train structure which extends from central Atlantic to Eurasia. It projects on the positive phase of the EA-WR pattern but also on the negative phase of the NAO. It resembles the sea level pressure pattern associated to the positive AMO phase [e.g., *Peings and Magnusdottir,* 2014]. Note that the main center of negative Z500 anomalies is located over the central North Atlantic Ocean. The PC2 is significantly positively correlated with EA-WR and negatively correlated with the NAO (Figure 5b). The negative correlation between AMO and NAO is reported also in *Peings and Magnusdottir* [2014]. The EA and SCA indices are not significantly correlated with PC2 blocking index, consistent with correlation pattern represented in Figure 5a.

To better assess and confirm that part of the AMO signal is presented in PC2 blocking pattern we performed a correlation analysis of 2-D blocking field based on AMO index. Both the blocking and the AMO indices were linearly detrended and filtered to retain the multidecadal variability (time scales longer than 20 years) before correlation analysis. Indeed, the blocking correlation map with AMO index (Figure 6a) resembles the second pattern of blocking variability (Figure 4a). However, it is difficult to assess the significance of these correlations due to low number of degrees of freedom. The correlation map of blocking PC2 and SST anomalies at multidecadal time scales shows a monopolar pattern with highest correlations in the subtropical region (Figure 6b). An SST index, defined as the average SST anomalies over (50°W–30°W; 10°N–20°N) region, where the correlations of PC2 and SST are the highest

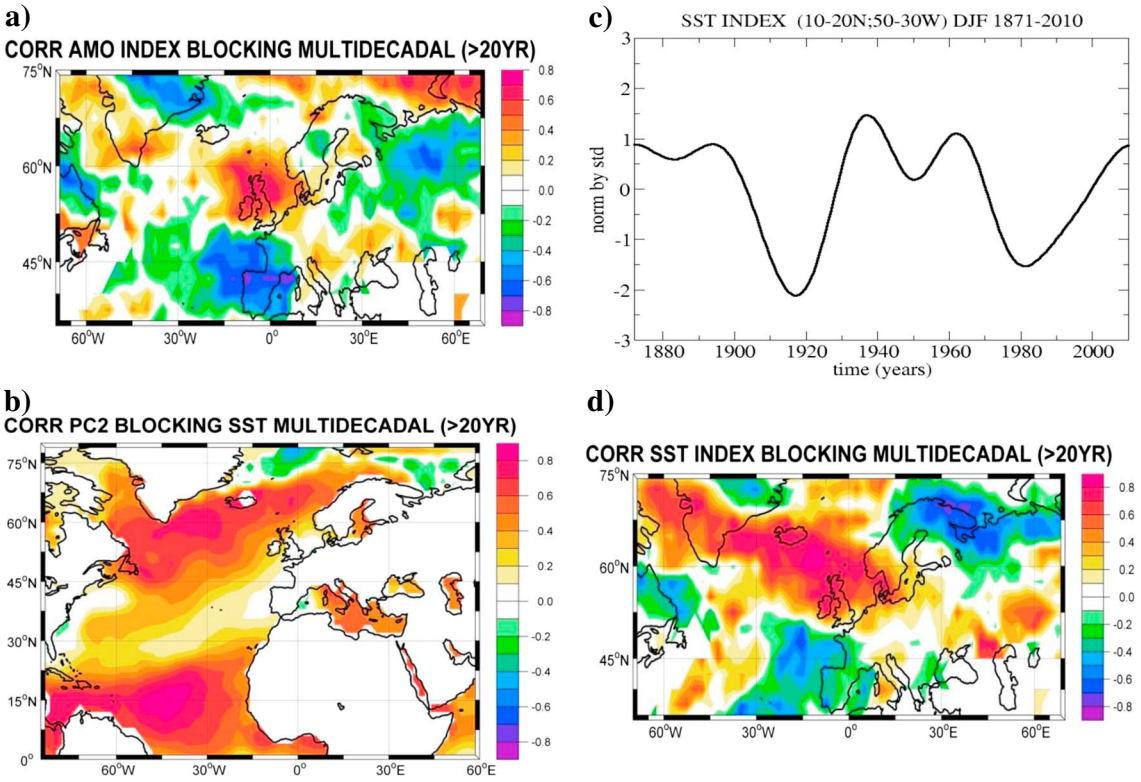

Figure 6. (a) The correlation map between AMO index and blocking frequency; (b) the correlation map of blocking PC2 and North Atlantic Ocean sea surface temperature (SST); (c) the time series of the SST index defined as the average of winter SST anomalies within (10°N–20°N; 50°W–30°W) region and (d) the correlation map between the SST index and the winter blocking frequency. The data are filtered in the multidecadal frequency band (time scales longer than 20 years). Period is 1871–2010.

(Figure 6b), follows variations similar to the AMO index but shows a more pronounced decrease in 1950s like the blocking index (Figure 6c). The correlation map of this SST index and blocking (Figure 6d) resembles also the blocking EOF2, but the correlations are higher relative to the corresponding AMO pattern (Figure 6a).

The third pattern of blocking variability (Figure 7a), which describes 7% of the total variance, captures mainly the out-of-phase variations in the Scandinavian and Greenland blocking frequency anomalies. It resembles the blocking anomaly pattern associated to the forth pattern of Z500 anomalies from the Atlantic-European region [*Scherrer et al.,* 2006, their Figure 8] which is closest to the SCA pattern. This blocking pattern resembles EOF3 of blocking anomalies from NCEP1 (Figure S4a) and EOF2 of ERA-40 (Figure S4b), consistent with significant positive correlations between the corresponding PCs (Figure S4c). This is confirmed by the composite analysis of classical 1-D TM index (Figure 7b) which shows relatively high (low) blocking activity in the (0°E–60°E) and (80°W–30°W) sectors during positive phases of this 2-D blocking pattern. The corresponding PC3 (Figure 7c) shows pronounced interannual but also decadal variations. PC3 is significantly (90% level) positively correlated ($r = +0.65$) with the time series of a regional blocking index defined as the difference in the normalized blocking frequency in the (0°E–60°E) and (80°W–30°W) sectors. The corresponding wavelet spectrum (Figure 7d) shows enhanced variability at ~20 years. The blocking PC3 and open solar flux time series, filtered in the 17–25 year frequency band, show out-of-phase variations over entire 1871–2010 period (Figure 7c, thick lines) with some delay. This is consistent with the correlation map of open solar flux and blocking in this frequency interval (Figure S5a) and also with sea level pressure pattern associated to solar insolation in this frequency interval [*Lohmann et al.,* 2004]. Furthermore, the composite map of 1-D blocking based on open solar flux time series in this frequency interval (Figure S5b) is similar with the composite map of blocking for high and low solar years as presented by *Barriopedro et al.* [2008]. These results are not sensitive to the exact choice of frequency band in which data are filtered or to filtering procedure.

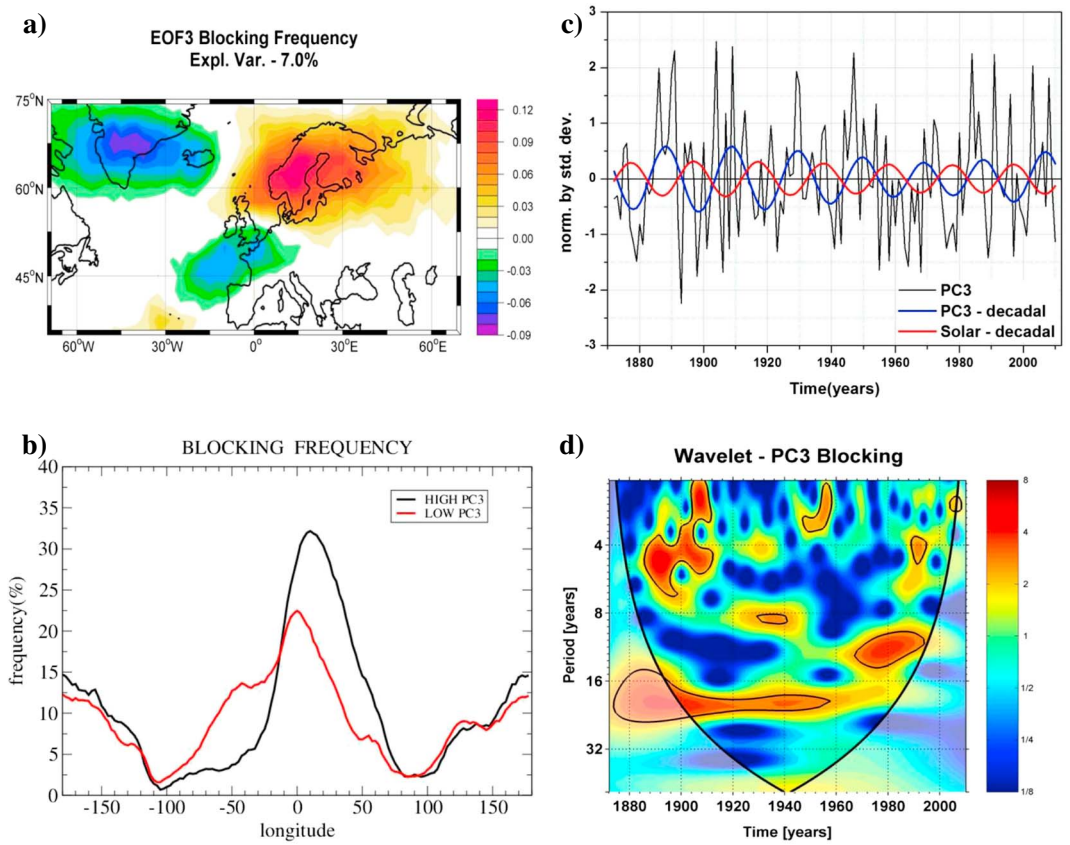

Figure 7. (a) The third EOF of blocking frequency variability; (b) blocking frequency associated to positive (black) and negative (red) phase of the pattern represented in a) as detected by one-dimensional TM index; (c) the corresponding PC3 (black). The thick blue (red) lines represent the PC3 (open solar flux) filtered in the 17–25 year frequency interval; (d) the continuous wavelet spectrum of PC3. The thick black contours designate the 90% significance level against white noise. The spectrum outside the cone of influence where the edge effects might be important is shown as a light shaded. Colors show power or variance.

The correlation map of blocking PC3 with Z500 (Figure 8a) shows a spatial structure similar to SCA pattern but contains also elements of NAO pattern. Consistent with the correlation map represented in Figure 8a, the PC3 is significantly (90%) positively correlated with SCA and NAO indices, but not significantly correlated with the EA and EA-WR indices, respectively (Figure 8b).

4. Relationship With Extreme Phenomena

Previous observational [*Trigo et al.*, 2004; *Cattiaux et al.*, 2010; *Silmann et al.*, 2011; *Pfahl and Wernli,* 2012; *Andrade et al.,* 2012] and modeling [e.g., *de Vries et al.,* 2013b] studies have demonstrated the existence of significant relationships between atmospheric blocking and extreme climate phenomena over Europe. In this respect, here, we investigate the extremely low temperature patterns associated to the dominant modes of 2-D blocking frequency variability described in the previous section. We identify these patterns using the correlation maps between blocking PCs and the TN10p indices. The TN10p indices are calculated from the gridded TN field extracted from the E-OBS data set, version 8.0, for the period 1950–2010. To check the robustness of the correlation patterns we analyze also the correlation maps of the blocking PCs and TN10p indices calculated using TN data as recorded at several meteorological stations distributed all over Europe. Figure 9a depicts the correlation map between winter blocking PC1 and the TN10p field over the European domain. The blocking PC1 is significantly positively correlated with TN10p indices over the northern Europe as well as significantly negatively correlated with TN10p indices over parts of Iberian Peninsula, Northern Africa, and southern Black Sea region (Figure 9a). The corresponding correlation pattern of PC1 with station-based indices (Figure 9d) shows a similar spatial structure. The highest positive (negative)

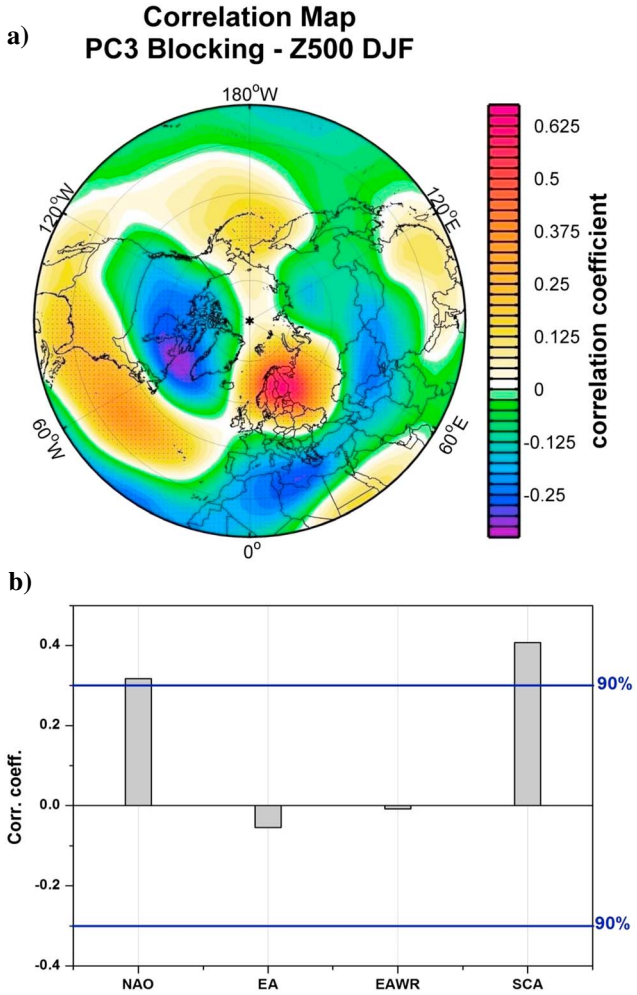

Figure 8. (a) Correlation map of winter blocking PC3 with Z500 for the period 1871–2010. The regions where correlation is above the 90% significance level are hatched; (b) the correlation coefficients between winter blocking PC3 and winter teleconnection indices for the period 1950–2010. Horizontal lines represent the 90% significance level.

correlations are recorded for the Baltic Sea area (Iberian Peninsula). The blocking PC2 is significantly positively correlated with TN10p indices from a south-west to north-east band from Europe (Figure 9b). The corresponding station based correlation map (Figure 9e) shows a similar spatial distribution of correlation coefficients. The highest correlations are recorded over the western part of Europe (Figure 9e). The blocking PC3 and TN10p field shows significant (90% level) positive correlations over a zonal band extending from Caspian Sea region to central Europe (Figure 9c). The corresponding station-based correlation map (Figure 9f) shows similar spatial structures, but correlations are higher over parts of Western Europe relative to the corresponding map based on gridded data (Figure 9c). Such differences could be related to quality of the data in early part of the records but also to instability of the teleconnections. A running correlation analysis (not shown) reveals important decadal variations of the correlation between blocking PCs and teleconnection patterns indices, especially for blocking PC2 and PC3.

The blocking PC2 (PC3) variations suggest a possible AMO (solar) influence on blocking variability at multidecadal (decadal) time scales. Therefore, these signals should be detected in the corresponding decadal to multidecadal patterns of TN10p variability. The correlation pattern of blocking PC2 and TN10p indices for decadal to multidecadal time scales (time scales longer than 7 years) (Figure 10a) is similar to the corresponding correlation pattern based on unfiltered data (Figure 9e). Also, the correlation pattern of blocking PC3 with TN10p indices at these time scales (Figure 10c) is similar to the corresponding correlation pattern based on unfiltered data (Figure 9f). To better assess and confirm the relationship between multidecadal variations of blocking, extremely low temperatures, and the AMO, we define an index by averaging the TN10p indices from all available stations from ECA&D data set within the (10°W–15°E; 42°N–47°N) region. This index is defined based on correlation map represented in Figure 10a. We identify eight records in the ECA&D data set which cover the period 1900–2010 and have less than 20% missing values. In this region correlation of PC2 with TN10p indices is relatively high comparative with the correlation of PC1 and PC3 (Figure 9). The resulting index is significantly positively correlated with PC2 over the period 1900–2010 ($r = +0.47$) when no filter is applied to the data. To focus on the AMO time scales the blocking PC2 and TN10p index are low-pass filtered to retain variations longer than 40 years. They are positively correlated with AMO index and the correlation is maximum when AMO leads both blocking PC2 and TN10p index with ~5–10 years (Figure 10b). This lead could be related to the response time of the atmosphere to the AMO forcing as in the case of the AMO impact on the NAO [*Peings and Magnusdottir*, 2014]. The fact that another phase of blocking multidecadal cycle maximizes the signal in the index region

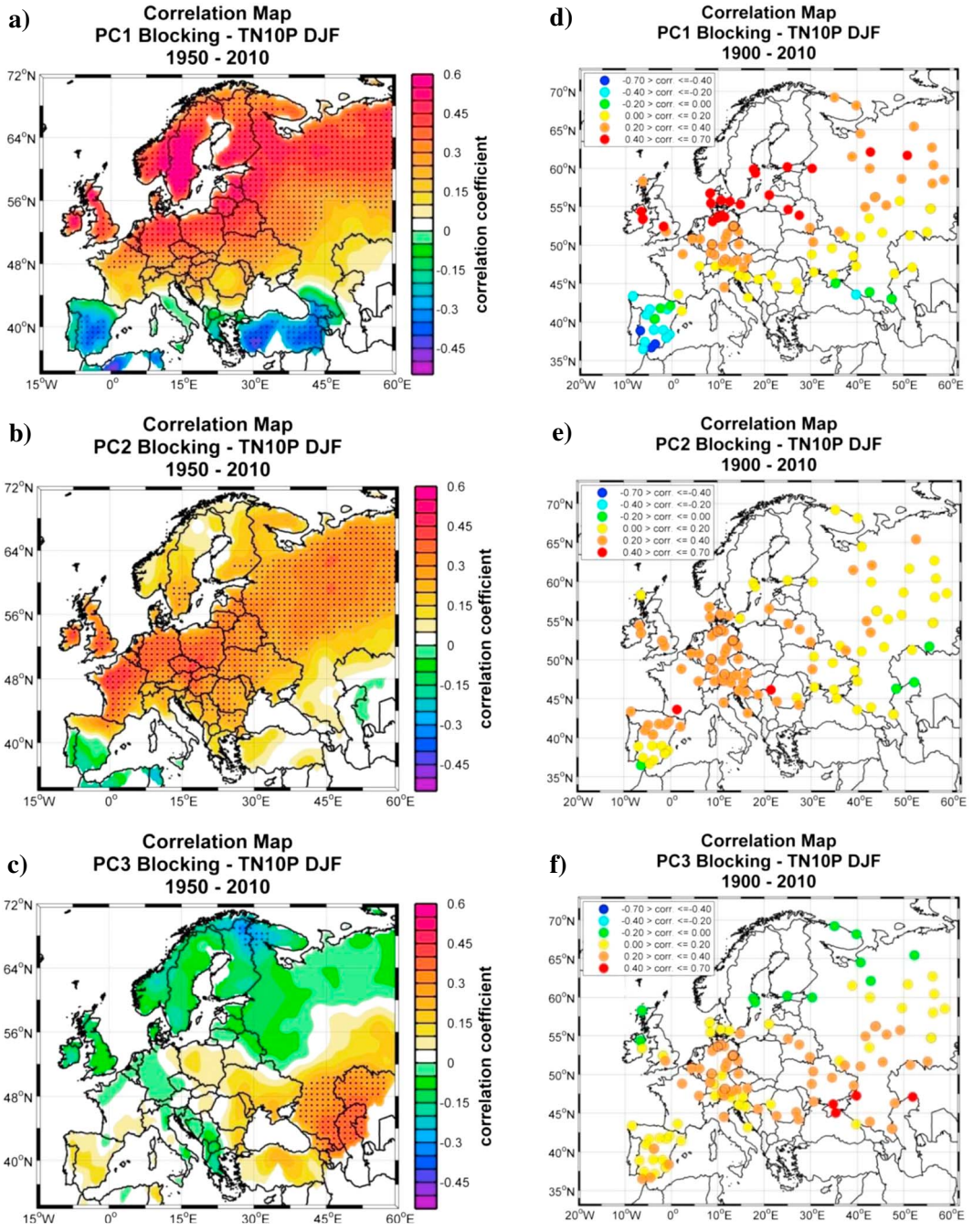

Figure 9. (a) The correlation map of blocking PC1 with the TN10p indices calculated from E-OBS gridded data set for the period 1950–2010. The regions where correlations are above 90% significance level are hatched; (d) the correlations of PC1 with TN10p indices derived using TN records from meteorological stations over Europe during the period 1900–2010 (see text for details); (b), (e) and (c), (f) as in Figures 9a and 9d but for PC2 and PC3, respectively.

could explain the lag time between the blocking PC2 and TN10p index time series at multidecadal time scales (Figure 10b).

Based on the correlation map of PC3 with TN10p field at decadal to multidecadal time scales (Figure 10c) we defined an index by averaging TN10p indices available from ECA&D within (30°E–50°E; 45°N–60°N). In this area the correlations of PC1 and PC2 with TN10p indices are relatively low. Twenty records from ECA&D satisfy the selection criteria. The resulting index (not shown) is significantly positively correlated with PC3 over the

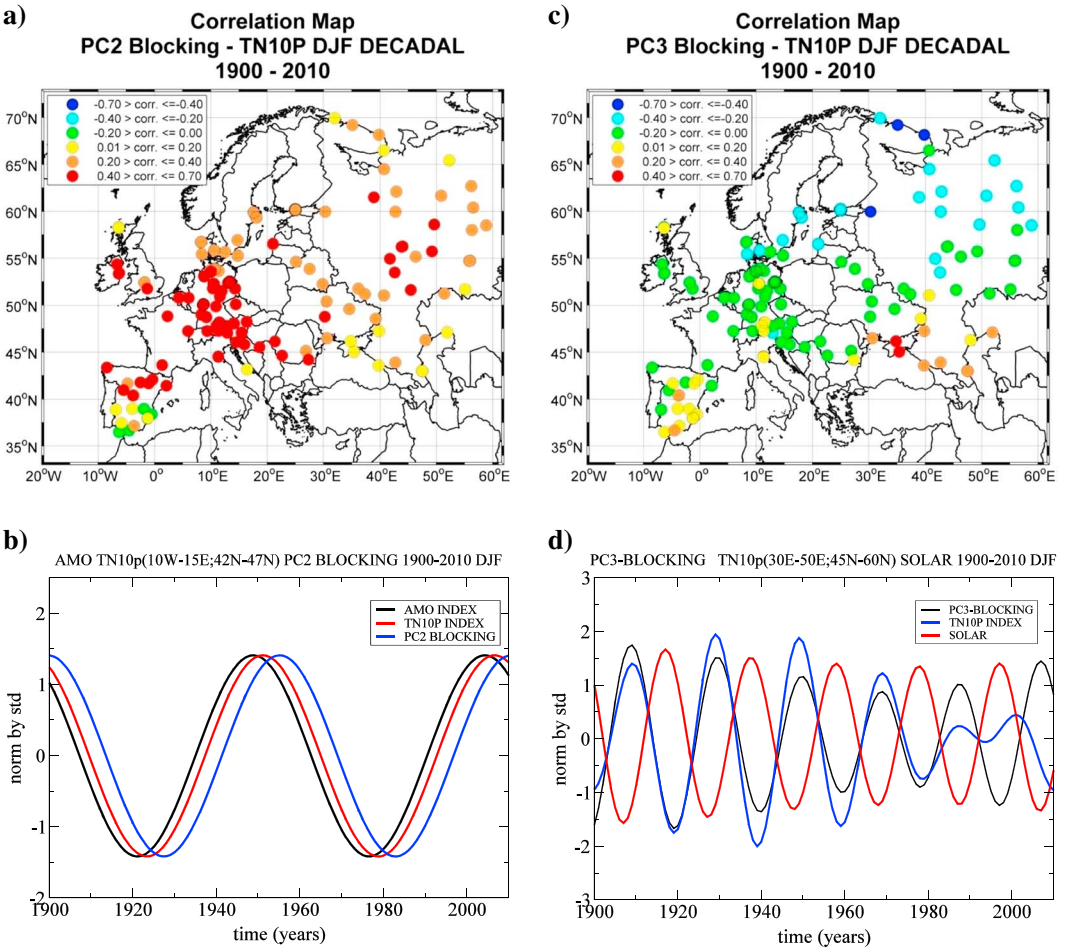

Figure 10. The correlations of decadal to multidecadal (time scales longer than 7 years) components of blocking (a) PC2 and (c) PC3 with TN10p indices during the period 1900–2010. (b) The multidecadal (time scales longer than 40 years) components of the AMO index (black), blocking PC2 (blue), and the average of TN10p indices over the area (10°W–15°E; 42°N–47°N) (red). (d) The decadal (17–25 year frequency interval) components of blocking PC3 (black), the open solar flux (red), and the average of TN10p indices over the area (30°E–50°E; 45°N–60°N) (blue).

period 1900–2011. The 17–25 year filtered components of the two indices (Figure 10d) show coherent variations over entire 1900–2010 period. However, a sensitivity study reveals that these variations are less coherent during last two decades, consistent with the wavelet spectrum represented in Figure 7d. The open solar flux shows out-of-phase variations with blocking and extreme temperature indices (Figure 10d).

5. Discussion and Conclusions

Traditionally, blocking variability is investigated using sectorial paradigm [e.g., *Barriopedro et al.,* 2006]. Here we used a complementary approach to investigate the relationship between blocking activity in different sectors. Multivariate analysis techniques were applied to a two-dimensional blocking frequency anomaly field and the dominant spatial and temporal patterns of variability were identified. Considering all time scales from interannual to multidecadal variability the first three patterns of blocking variability resemble the corresponding blocking patterns associated to EOF1, EOF3, and EOF4 of winter Z500 anomalies from the North Atlantic region as derived by *Scherrer et al.* [2006] which are closest to the NAO, EA-WR, and SCA patterns. However, the blocking patterns, identified in our study through an EOF analysis of blocking anomaly field over relatively long period, are significantly correlated with several teleconnection patterns, up to four.

The first three patterns of unfiltered blocking anomaly field, identified in our study, describe only 35% variance. If the blocking data are filtered in the decadal band (7 to 20 year) the blocking patterns as well as the

corresponding TN10p patterns remain qualitatively the same (not shown) but the described variance increases to 44%. Therefore, a substantial part of the blocking variability, both at interannual and decadal time scales, remains to be explained by other patterns. When blocking field is filtered in the multidecadal band (time scale longer than 20 year) the first EOF, which describes 22% variance (Figure S6a), has a spatial structure similar with EOF2 of unfiltered (Figure 4a) blocking anomaly field. The corresponding PC (Figure S6b) is practically identical with the multidecadal component of PC2 of unfiltered blocking data (Figure 4c). Therefore, also in this case, a large part of multidecadal blocking variability in the North Atlantic region remains to be described by other patterns.

The relatively long time series of the principal components associated to the dominant pattern of blocking variability presented here (i.e., 140 years) open the possibility to investigate the decadal to multidecadal variations of blocking activity in the North Atlantic as well as the corresponding teleconnections. The wavelet spectrum of blocking PC1 resembles the corresponding NAO wavelet spectrum [*Walter and Graf,* 2002]. As in the case of the NAO, PC1 shows fluctuations with periods around 16 years from 1900 to 1920, around 12 years from 1920 to 1940 as well as two other peaks for periods around 16 and 8 years from 1965/1970 to 2000. The second blocking pattern, which captures mainly the variability of the classical blocking events [*Trigo et al.,* 2004], shows multidecadal variations similar to the AMO. The coherent variations of blocking PC2 and AMO index suggest an AMO influence on blocking variability at these time scales. It was shown [*Häkkinen et al.,* 2011] that enhanced blocking activity in a region stretching from Greenland to western Europe is related to a warmer and more saline subpolar Atlantic Ocean as well as with warmer Atlantic tropical and subtropical region. *Häkkinen et al.* [2011] argue that wind forcing associated to this pattern of blocking variability leads to weaker ocean gyres and weaker heat exchange between ocean and the atmosphere, which contribute to the increased temperature over much of the North Atlantic Ocean. This suggests, that at least the multidecadal blocking variability, as captured by the second blocking EOF, is related to atmosphere-ocean interaction processes from the North Atlantic. The ~30 year oscillation emphasized in the blocking PC2 wavelet spectrum in the 1920 to 1980 period is in phase with subtropical Atlantic SST anomalies, suggesting a possible connection between them. Therefore, the relationship between multidecadal (time scales longer than 20 years) blocking and SST variations is a complex one, and further research is needed to clarify the relationship between the AMO and blocking EOF2. The third pattern of blocking variability shows a persistent oscillation at about 20 years. The 20 years oscillation was already reported in previous studies to be a dominant mode of blocking variability [*Rimbu et al.,* 2007; *Rimbu and Lohmann,* 2011]. This oscillation could be related to the variability in the solar activity. It was shown [*Woollings et al.,* 2010] that during high (low) solar winters, as derived using open solar flux calculated based on geomagnetic data, low (high) blocking activity is recorded over a broad region extended from central Atlantic to Eurasian sector as well as high (low) blocking activity over Greenland (their Figure 4). Their blocking pattern captures also the out-of-phase variations of blocking frequency between Greenland and Europe as our blocking EOF3. Negative (positive) sea level pressure (SLP) anomalies over Greenland (UK to Scandinavia region), which are indicative of low (high) blocking frequency in these regions, are emphasized on the map of difference between composite SLP corresponding to low and high solar irradiance as simulated by a climate model [*Moffa-Sánchez et al.,* 2014]. This is consistent with out-of-phase variations of the 20 year oscillation identified in blocking PC3 and open solar flux as presented in our study. A correlation analysis between open solar flux and blocking field (Figure S5) reveals also that Greenland and Scandinavian blocking are out-of-phase at these time scales. However, the solar related blocking pattern presented in Figure S5a is consistent with *Woollings et al.* [2010] blocking pattern and *Moffa-Sánchez et al.* [2014] SLP anomaly pattern but shows more pronounced solar impact on continental area like our EOF3. These differences could be related to different time scales considered in our study.

The 2-D blocking indicator used in this study [*Scherrer et al.,* 2006] does not consider any spatial criteria. Therefore, the analysis presented in this study can be extended to the analysis of more complex blocking indices. However, preliminary results show that the blocking patterns described in this study remain qualitatively the same when both spatial and temporal criteria are considered in the 2-D blocking index definition. This is consistent with *Davini et al.* [2012] which show that the distribution of instantaneous blocking frequency is only slightly affected by the introduction of spatial and temporal constraints in blocking frequency calculation (their Figure 1).

Blocking events appear in different geographic locations and are governed by different mechanisms and have specific impact. The blocking occurring at midlatitudes blocks the west to east flow and has strong impact on extreme weather events. Low-latitude blocking, occurring south of 40°N, is unable to block or even to divert the flow [*Davini et al.,* 2012]. *Masato et al.* [2013] show that midlatitude blocking is observed over Europe and Asia whereas high-latitude blocking is mainly present over the oceans. Therefore, we investigate if the blocking patterns, as presented in our study, are dependent on the modification of latitudinal domain used in the EOF analysis. Our results show that both spatial patterns (Figure S7) and the corresponding time coefficients (not shown) are not sensitive to the modification of latitudinal extent of the spatial domain. We may conclude that the patterns presented in our study represent stable characteristics of interannual to multidecadal blocking variability in the Atlantic-European region.

We have shown that the dominant patterns of blocking variability have a specific impact on extreme low temperature variability. The first blocking pattern induces a north-south dipole in the anomalous occurrence of extremely low temperatures. Blocking associated to the positive phase of this pattern is related to enhanced advection of very cold air from the polar region towards northern Europe. The second pattern of blocking induces cold events over the entire Europe. The third pattern induces cold events over continental region, especially Black Sea-Caspian Sea region. These patterns remain qualitatively the same for interannual to decadal time scales. We suggest that multidecadal variations in the frequency of extreme temperature events from a region extending from southwestern to northeastern Europe, which have also an ~70 year time scales, are induced by the AMO related blocking pattern via advection of cold air masses from the north. This is consistent with AMO impact on frequency on weather regimes and related extreme temperatures in Europe as derived from observations and model experiments [*Peings and Magnusdottir,* 2014]. The ~20 year oscillation in the frequency of cold events over southeastern Europe could be related to solar activity, which modulates the blocking frequency in the Atlantic European region. Low solar radiation, enhanced nighttime radiative cooling due to reduced cloudiness, together with cold advection associated to high blocking activity over these regions could generate extreme low temperatures over southern Europe, consistent with out-of-phase variations of TN10p index associated to extremely low temperatures in these regions and open solar flux, as shown here.

The multivariate analysis of a two-dimensional blocking indicator, as presented in this study, reveals new characteristics of spatial and temporal blocking variability and predictability in the North Atlantic region and related extreme climatic phenomena over Europe. The relatively small influence of the AMO or solar forcing on blocking variability was clearly identified based on this approach. However, the physical mechanisms responsible for blocking variability and predictability at interannual to multidecadal time scales should be investigated further using more complex blocking indices as well as various multivariate methods.

Acknowledgments

The work was supported by REKLIM project. We acknowledge the use of the 20CR (/www.esrl.noaa.gov/psd/data/gridded/data.20thC-ReanV2.html), NCEP1 (www.esrl.noaa.gov/psd/data/gridded/data.ncep.reanalysis.html), and ERA-40 (www.ecmwf.int/products/data/arcchive) reanalysis data sets, sea surface temperature ERSST.v3b (www.esrl.noaa.gov/psd/data/gridded/data.noaa.esst.html), and gridded daily data set E-OBS (http://www.ecad.eu/download/ensembles/ensembles.php). We acknowledge also the use of the following time series: indices of extreme temperature (ECA&D) (www.ecad.eu/download/millennium/millennium.php), teleconnection indices (www.cpc.ncep.noaa.gov), AMO (www.esrl.noaa.gov/psd/data/timeseries/AMO/), NAO (https://climatedataguide.ucar.edu/climate-data/hurrell-north-atlantic-oscillation-nao-index-pc-based) as well as open solar flux (http://climexp.knmi.nl/data/iosfa.txt). We thank the four anonymous reviewers for their constructive comments that significantly improved the manuscript.

References

Andrade, C., M. Leite, and J. A. Santos (2012), Temperature extremes in Europe: overview of their driving atmospheric patterns, *Nat. Hazards Earth Syst. Sci.*, *12*, 671–1691, doi:10.5194/nhess-12-1671-2012.

Barnes, A. E., E. Dunn-Sigouin, G. Masato, and T. Woollings (2014), Exploring recent trends in Northern Hemisphere blocking, *Geophys. Res. Lett.*, *41*, 638–644, doi:10.1002/2013GL058745.

Barriopedro, D., R. García-Herrera, A. R. Lupo, and E. Hernandez (2006), A climatology of Northern Hemisphere blocking, *J. Clim.*, *19*, 1042–1063.

Barriopedro, D., R. García-Herrera, and R. Huth (2008), Solar modulation of Northern Hemisphere winter blocking, *J. Geophys. Res.*, *113*, D14118, doi:10.1029/2008JD009789.

Barriopedro, D., R. G. Herrera, and R. M. Trigo (2010), Application of blocking diagnosis methods to General CirculationModels. Part I: A novel detection scheme, *Clim. Dyn.*, *35*, 1373–1391, doi:10.1007/s00382-010-0767-5.

Cattiaux, J., R. Vautard, C. Cassou, P. Yiou, V. Masson-Delmotte, and F. Codron (2010), Winter 2010 in Europe: A cold extreme in a warming climate, *Geophys. Res. Lett.*, *37*, L20704, doi:10.1029/2010GL044613.

Chen, T.-S., and J.-H. Yoon (2002), Interdecadal variation in the North Pacific wintertime blocking, *Mon. Weather Rev.*, *130*, 3136–3143.

Cheung, H., W. Zhou, H. Y. Mok, M. C. Wu, and Y. Shao (2013), Revisiting the climatology of atmospheric blocking in the Northern Hemisphere, *Adv. Atmos. Sci.*, *30*(2), 397–410.

Comas-Bru, L., and F. McDermott (2013), Impacts of the EA and SCA patterns on the European twentieth century NAO–winter climate relationship, *Q. J. R. Meteorol. Soc.*, *140*, 354–363, doi:10.1002/qj.2158.

Compo, G., et al. (2011), The twentieth century reanalysis project, *Q. J. R. Meteorol. Soc.*, *137*, 1–28, doi:10.1002/qj.776.

Croci-Maspoli, M., C. Schwierz, and H. C. Davies (2007), Atmospheric blocking: spacetime links to the NAO and PNA, *Clim. Dyn.*, *29*, 713–725, doi:10.1007/s00382-007-0259-4.

Davini, P., C. Cagnazzo, S. Gualdi, and A. Navarra (2012), Bidimensional diagnostics, variability and trends of Northern Hemisphere blocking, *J. Clim.*, *25*, 6496–6509.

de Vries, H., T. Woollings, and J. Anstey (2013a), Atmospheric blocking and its relation to jet changes in a future climate, *Clim. Dyn.*, *41*, 2643–2654, doi:10.1007/s00382-013-1699-7.

de Vries, H., R. J. Haarsma, and W. Hazeleger (2013b), On the future reduction of snowfall in western and central Europe, *Clim. Dyn.*, *41*, 2319–2330, doi:10.1007/s00382-012-1538-x.
Diao, Y., J. Li, and D. Luo (2006), A new blocking index and its application: blocking action in the Northern Hemisphere, *J. Clim.*, *19*, 4819–4839.
Dunn-Sigouin, E., and S.-W. Son (2013), Northern Hemisphere blocking frequency and duration in the CMIP5 models, *J. Geophys. Res. Atmos.*, *118*, 1179–1188, doi:10.1002/jgrd.50143.
Häkkinen, S., P. B. Rhines, and D. L. Worthen (2011), Atmospheric blocking and Atlantic multidecadal ocean variability, *Science*, *4*(334), 655–659, doi:10.1126/science.1205683.
Kalnay, E., et al. (1996), The NCEP/NCAR 40-Year Reanalysis Project, *Bull. Am. Meteorol. Soc.*, *77*, 437–471, doi:10.1175/1520-0477.
Klein Tank, A. M. G., et al. (2002), Daily data set of 20th-century surface air temperature and precipitation series for the European Climate Assessment, *Int. J. Climatol.*, *22*, 1441–1453.
Lockwood, M. A., P. Rouillard, and D. Finch (2009), The rise and fall of open solar flux during the current grand solar maxumum, *Astrophys. J.*, *700*, 937–944.
Lohmann, G., N. Rimbu, and M. Dima (2004), Climate signature of solar irradiance variations: analysis of long-term instrumental, historical, and proxy data, *Int. J. Climatol.*, *24*, 1045–1056, doi:10.1002/joc.1054.
Masato, G., B. J. Hoskins, and T. Woollings (2013), Wave-breaking characteristics of Northern Hemisphere winter blocking: a two-dimensional approach, *J. Clim.*, *26*, 4535–4549, doi:10.1175/JCLI-D-12-00240.1.
Moffa-Sánchez, P., A. Born, I. R. Hall, D. J. R. Thornalley, and S. Barker (2014), Solar forcing of North Atlantic surface temperature and salinity over the past millennium, *Nat. Geosci.*, *7*, 275–278, doi:10.1038/NGEO2094.
North, R. G., T. L. Dell, F. Cahalan, and F. J. Moeng (1982), Sampling errors in the estimation of Empirical Orthogonal Functions, *Mon. Weather Rev.*, *110*, 699–706.
Peings, Y., and G. Magnusdottir (2014), Response of the wintertime northern hemisphere atmospheric circulation to current and projected Arctic Sea Ice decline: A numerical study with CAM5, *J. Clim.*, *27*, 244–264.
Pfahl, S., and H. Wernli (2012), Quantifying the relevance of atmospheric blocking for co-located temperature extremes in the Northern Hemisphere on (sub-) daily time scales, *Geophys. Res. Lett.*, *39*, L12807, doi:10.1029/2012GL052261.
Rimbu, N., and G. Lohmann (2011), Winter and summer blocking variability in the North Atlantic region. Evidence from long-term observational and proxy data from southwestern Greenland, *Clim. Past*, *7*, 543–555.
Rimbu, N., G. Lohmann, and K. Grosfeld (2007), Northern Hemisphere atmospheric blocking in ice core accumulation records from northern Greenland, *Geophys. Res. Lett.*, *34*, L09704, doi:10.1029/2006GL029175.
Scherrer, S., M. Croci-Maspoli, C. Schwierz, and C. Appenzeller (2006), Two-dimensional indices of atmospheric blocking and their statistical relationship with winter climate patterns in the Euro-Atlantic region, *Int. J. Climatol.*, *26*, 233–249, doi:10.1002/joc.1250.
Shabbar, A., J. Huang, and K. Higuchi (2001), The relationship between the wintertime North Atlantic Oscillation and blocking episodes in the North Atlantic, *Int. J. Climatol.*, *21*, 355–369.
Silmann, J., and M. Croci-Maspoli (2009), Present and future atmospheric blocking and its impact on European mean and extreme climate, *Geophys. Res. Lett.*, *36*, L10702, doi:10.1020/2009GL038259.
Silmann, J., M. Croci-Maspoli, M. Kallache, and R. W. Katz (2011), Extreme cold winter temperatures in Europe under the influence of North Atlantic atmospheric blocking, *J. Clim.*, *24*, 5899–5913, doi:10.1175/2011JCLI4075.1.
Smith, T. M., R. W. Reynolds, C. Peterson, and J. Lawrimore (2008), Improvements NOAAs historical merged land-ocean temperature analysis (1880-206), *J. Clim.*, *21*, 2283–2296.
Tibaldi, S., and F. Molteni (1990), On the operational predictability of blocking, *Tellus A*, *42*, 343–365.
Torrence, C., and G. P. Compo (1998), A Practical Guide to Wavelet Analysis, *Bull. Am. Meteorol. Soc.*, *79*, 6178, doi:10.1175/1520-0477.
Trigo, R. M., I. M. Trigo, C. C. DaCamara, and T. J. Osborn (2004), Climate impact of the European winter blocking episodes from the NCEP/NCAR Reanalyses, *Clim. Dyn.*, *23*(1), 17–28.
Uppala, S. M., et al. (2005), The ERA-40 Re-Analysis, *Q. J. R. Meteorol. Soc.*, *131*, 2961–3012.
van den Besselaar, E. J. M., M. R. Haylock, G. van der Schrier, and A. M. G. Klein Tank (2011), A European Daily High-resolution Observational Gridded Data set of Sea Level Pressure, *J. Geophys. Res.*, *116*, D11110, doi:10.1029/2010JD015468.
von Storch, H., and F. W. Zwiers (1999), *Statistical Analysis in Climate Research*, pp. 494, Cambridge Univ. Press, Cambridge, U. K.
Walter, K., and H.-F. Graf (2002), On the changing nature of the regional connection between the North Atlantic Oscillation and sea surface temperature, *J. Geophys. Res.*, *107*(D17), 4338, doi:10.1029/2001JD000850.
Woollings, T., and M. Blackburn (2012), The North Atlantic jet stream under climate change and its relation to the NAO and EA patterns, *J. Clim.*, *25*, doi:10.1175/JCLI-D-11-00087.1.
Woollings, T., M. Lockwood, G. Masato, C. Bell, and L. Gray (2010), Enhanced signature of solar variability in Eurasian winter climate, *Geophys. Res. Lett.*, *37*, L20805, doi:10.1029/2010GL044601.

a)

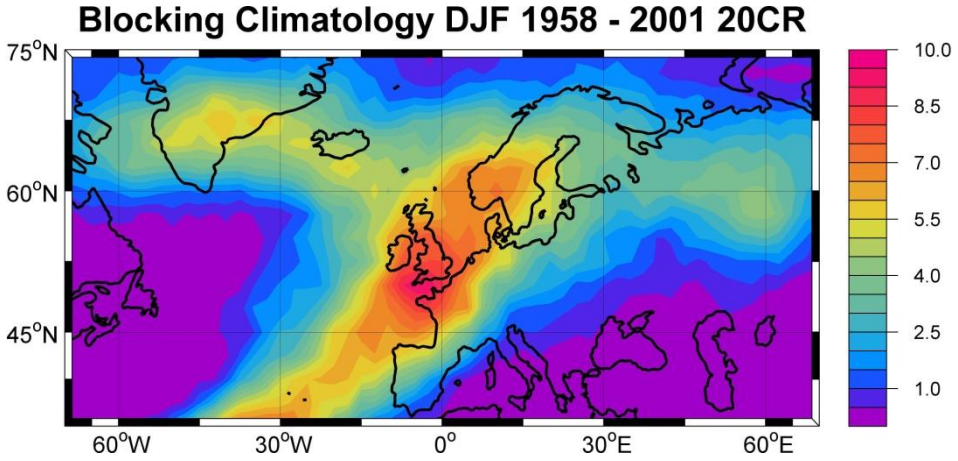
Blocking Climatology DJF 1958 - 2001 20CR
75°N
60°N
45°N
60°W
30°W
0°
30°E
60°E
10.0
8.5
7.0
5.5
4.0
2.5
1.0

b)

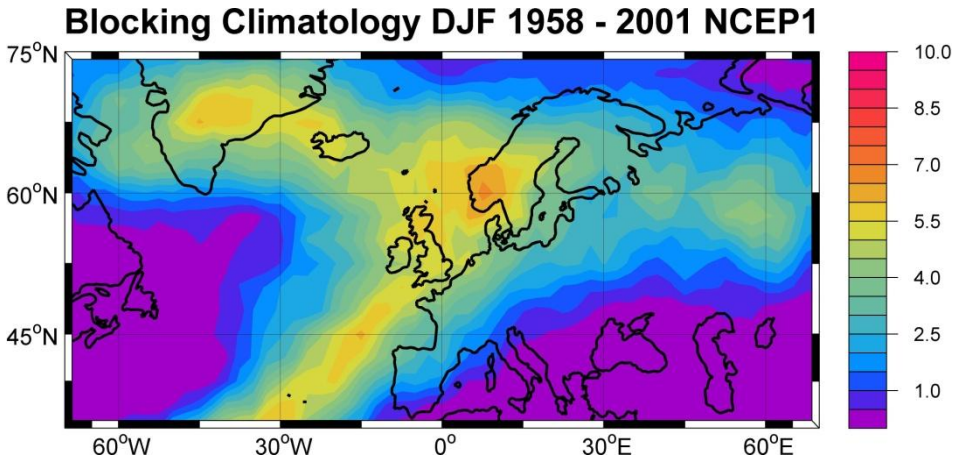
Blocking Climatology DJF 1958 - 2001 NCEP1
75°N
60°N
45°N
60°W
30°W
0°
30°E
60°E
10.0
8.5
7.0
5.5
4.0
2.5
1.0

c)

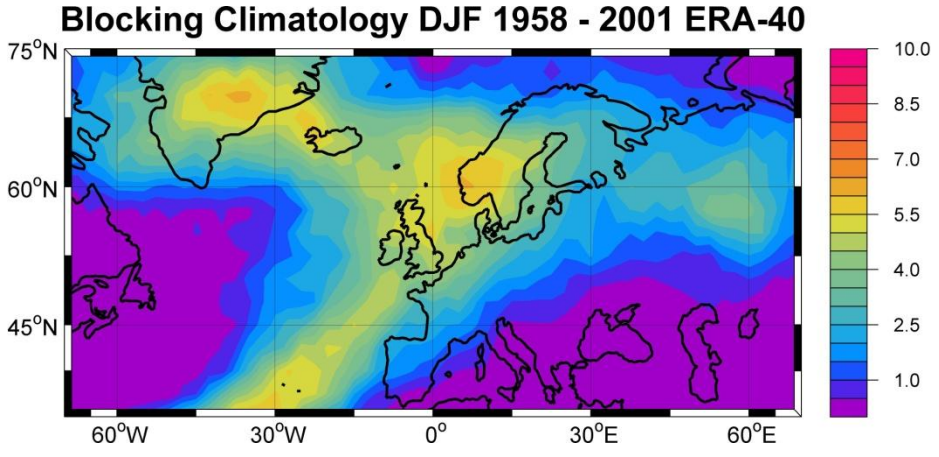
Blocking Climatology DJF 1958 - 2001 ERA-40
75°N
60°N
45°N
60°W
30°W
0°
30°E
60°E
10.0
8.5
7.0
5.5
4.0
2.5
1.0

a)

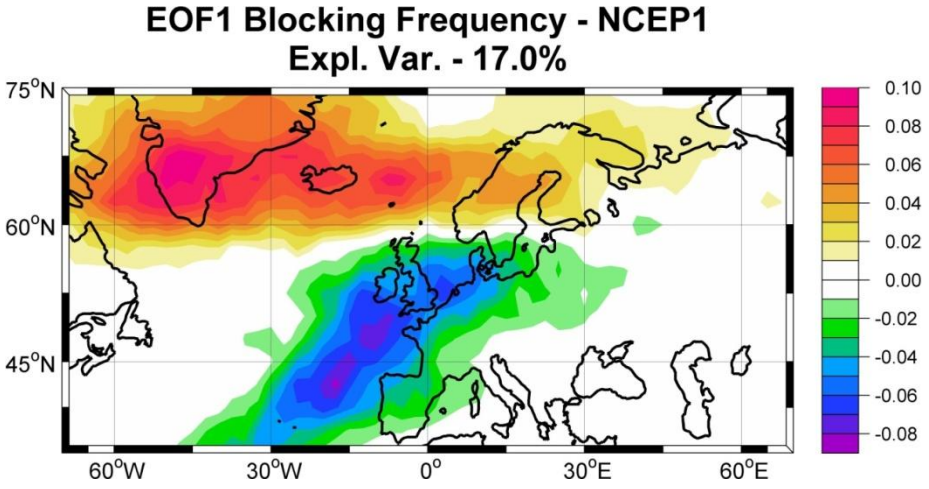
EOF1 Blocking Frequency - NCEP1
Expl. Var. - 17.0%
75°N
60°N
45°N
60°W
30°W
0°
30°E
60°E
0.10
0.08
0.06
0.04
0.02
0.00
-0.02
-0.04
-0.06
-0.08

b)

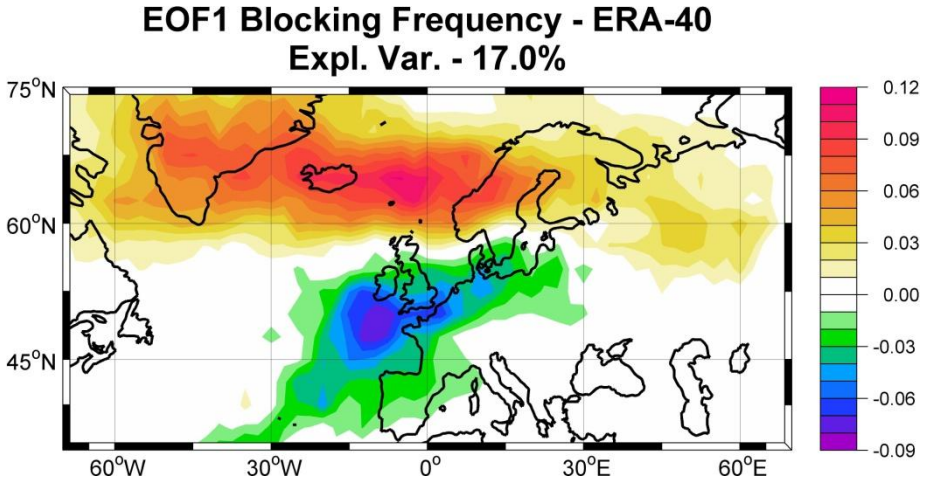
EOF1 Blocking Frequency - ERA-40
Expl. Var. - 17.0%
75°N
60°N
45°N
60°W
30°W
0°
30°E
60°E
0.12
0.09
0.06
0.03
0.00
-0.03
-0.06
-0.09

c)

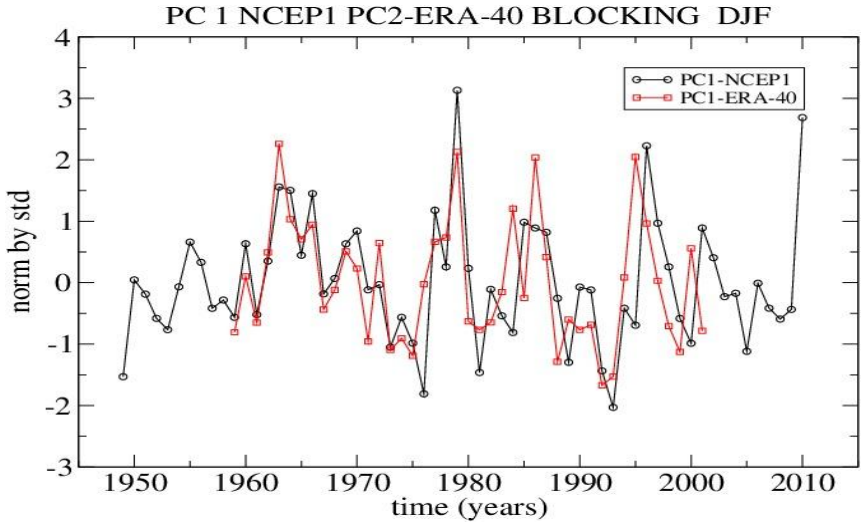
PC 1 NCEP1 PC2-ERA-40 BLOCKING DJF
PC1-NCEP1
PC1-ERA-40
norm by std
4
3
2
1
0
-1
-2
-3
1950
1960
1970
1980
1990
2000
2010
time (years)

a)

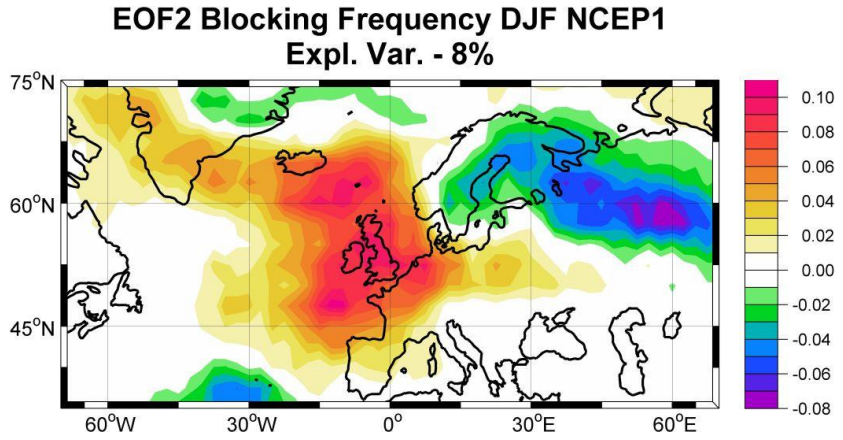
EOF2 Blocking Frequency DJF NCEP1
Expl. Var. - 8%
75°N
60°N
45°N
60°W
30°W
0°
30°E
60°E
0.10
0.08
0.06
0.04
0.02
0.00
-0.02
-0.04
-0.06
-0.08

b)

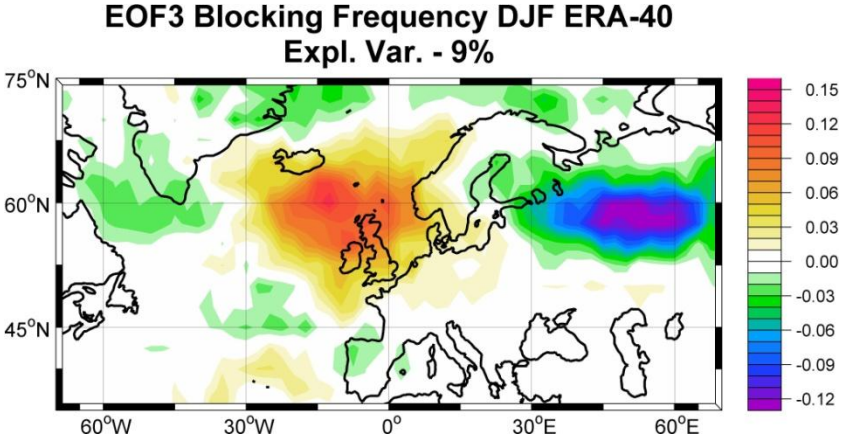
EOF3 Blocking Frequency DJF ERA-40
Expl. Var. - 9%
75°N
60°N
45°N
60°W
30°W
0°
30°E
60°E
0.15
0.12
0.09
0.06
0.03
0.00
-0.03
-0.06
-0.09
-0.12

c)

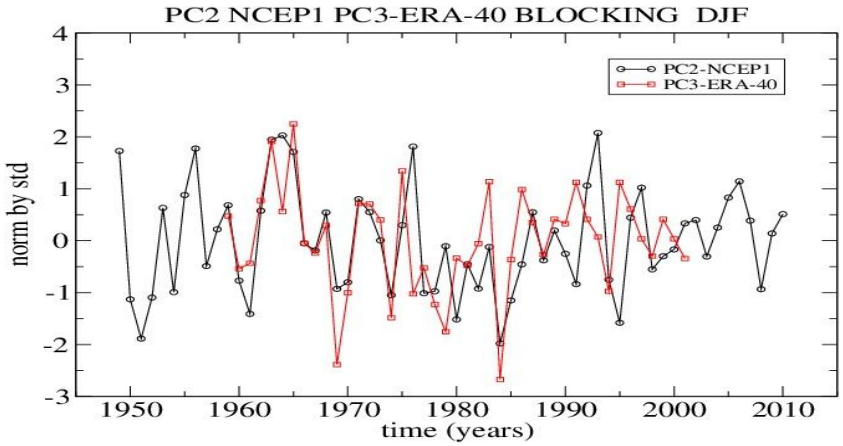
PC2 NCEP1 PC3-ERA-40 BLOCKING DJF
PC2-NCEP1
PC3-ERA-40
norm by std
4
3
2
1
0
-1
-2
-3
1950
1960
1970
1980
1990
2000
2010
time (years)

a)

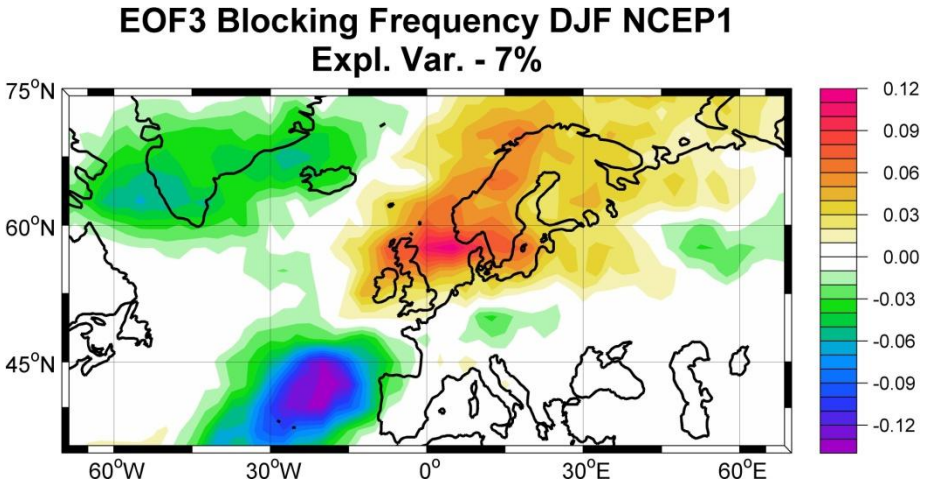
EOF3 Blocking Frequency DJF NCEP1
Expl. Var. - 7%
75°N
60°N
45°N
60°W
30°W
0°
30°E
60°E
0.12
0.09
0.06
0.03
0.00
-0.03
-0.06
-0.09
-0.12

b)

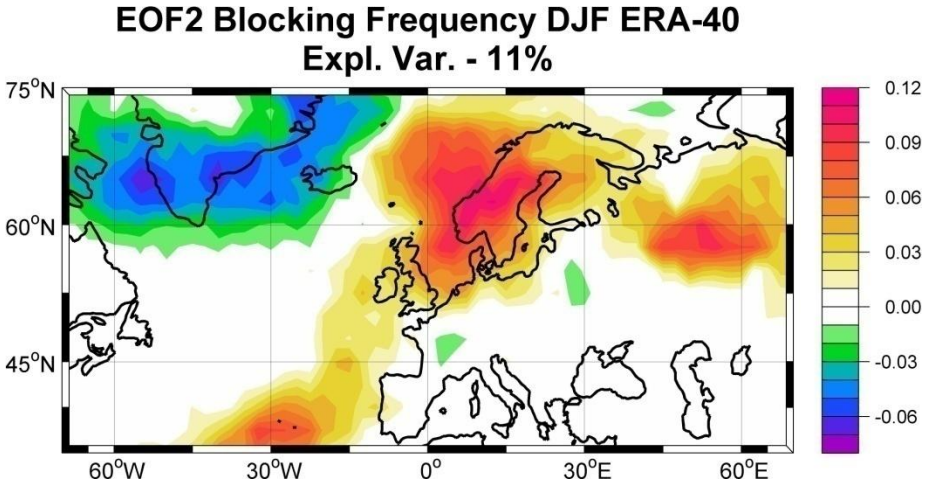
EOF2 Blocking Frequency DJF ERA-40
Expl. Var. - 11%
75°N
60°N
45°N
60°W
30°W
0°
30°E
60°E
0.12
0.09
0.06
0.03
0.00
-0.03
-0.06

c)

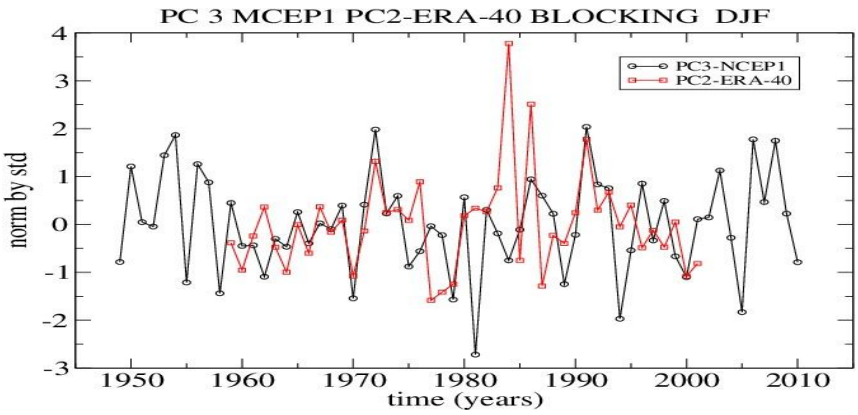
PC 3 MCEP1 PC2-ERA-40 BLOCKING DJF
PC3-NCEP1
PC2-ERA-40
norm by std
4
3
2
1
0
-1
-2
-3
1950
1960
1970
1980
1990
2000
2010
time (years)

a)

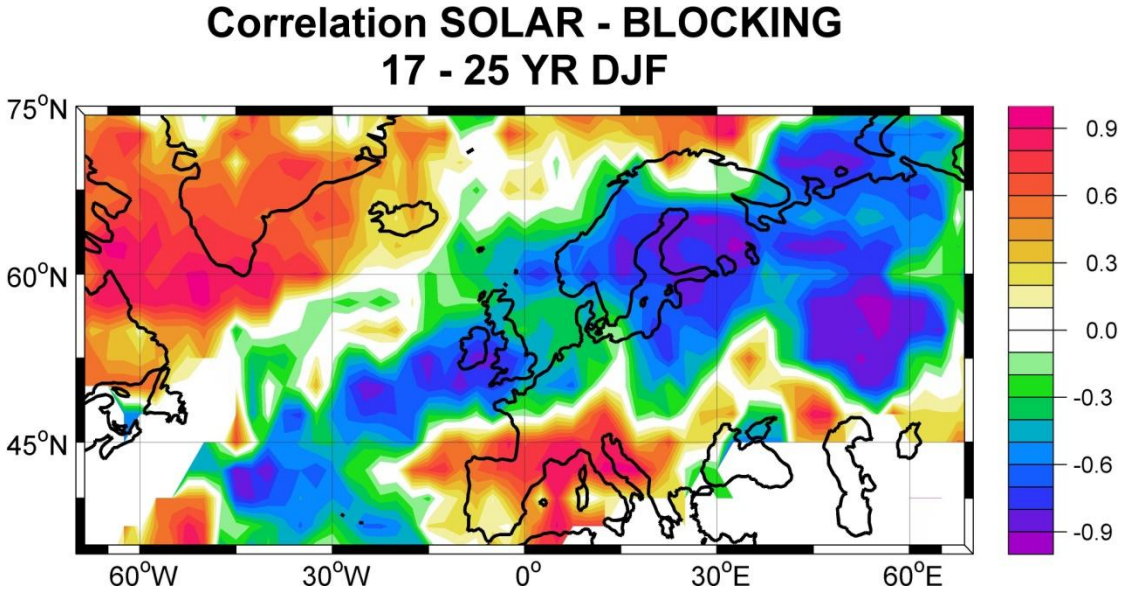
Correlation SOLAR - BLOCKING
17 - 25 YR DJF
75°N
60°N
45°N
60°W
30°W
0°
30°E
60°E
0.9
0.6
0.3
0.0
-0.3
-0.6
-0.9

b)

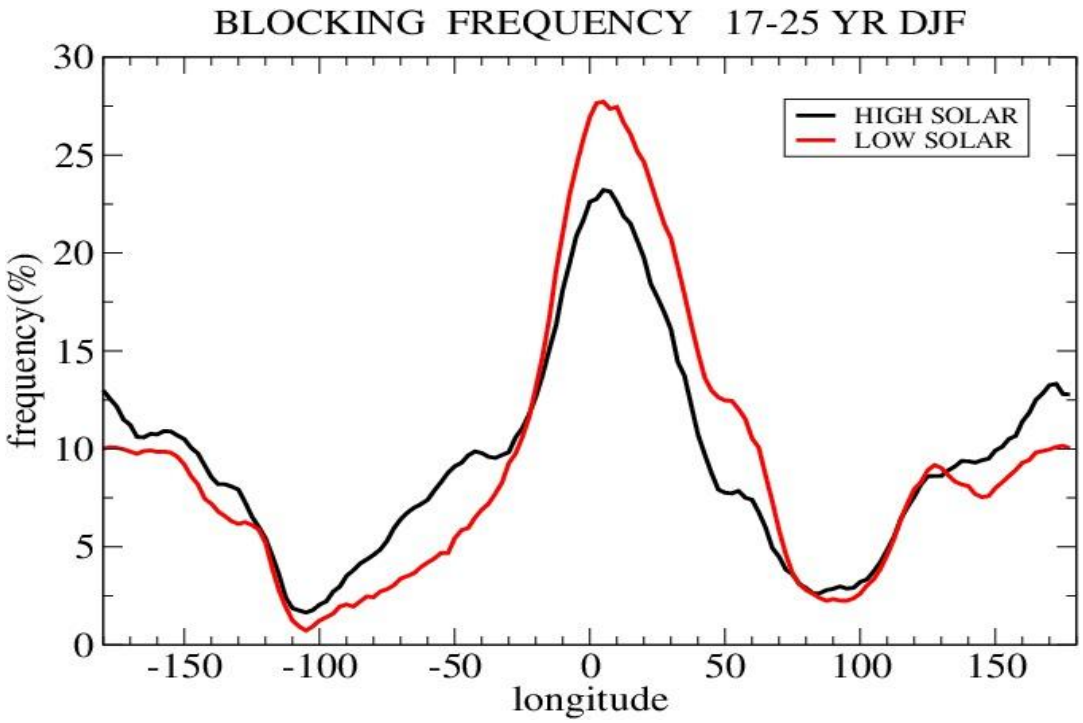
BLOCKING FREQUENCY 17-25 YR DJF
HIGH SOLAR
LOW SOLAR
frequency(%)
longitude
30
25
20
15
10
5
0
-150
-100
-50
0
50
100
150

a)

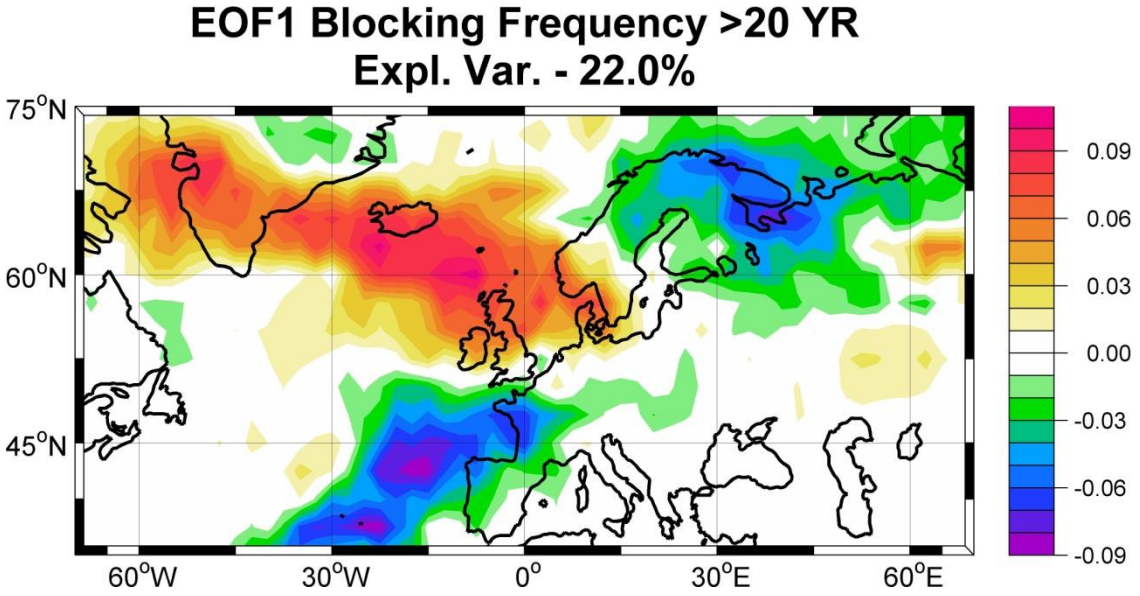
EOF1 Blocking Frequency >20 YR
Expl. Var. - 22.0%
75°N
60°N
45°N
60°W
30°W
0°
30°E
60°E
0.09
0.06
0.03
0.00
-0.03
-0.06
-0.09

b)

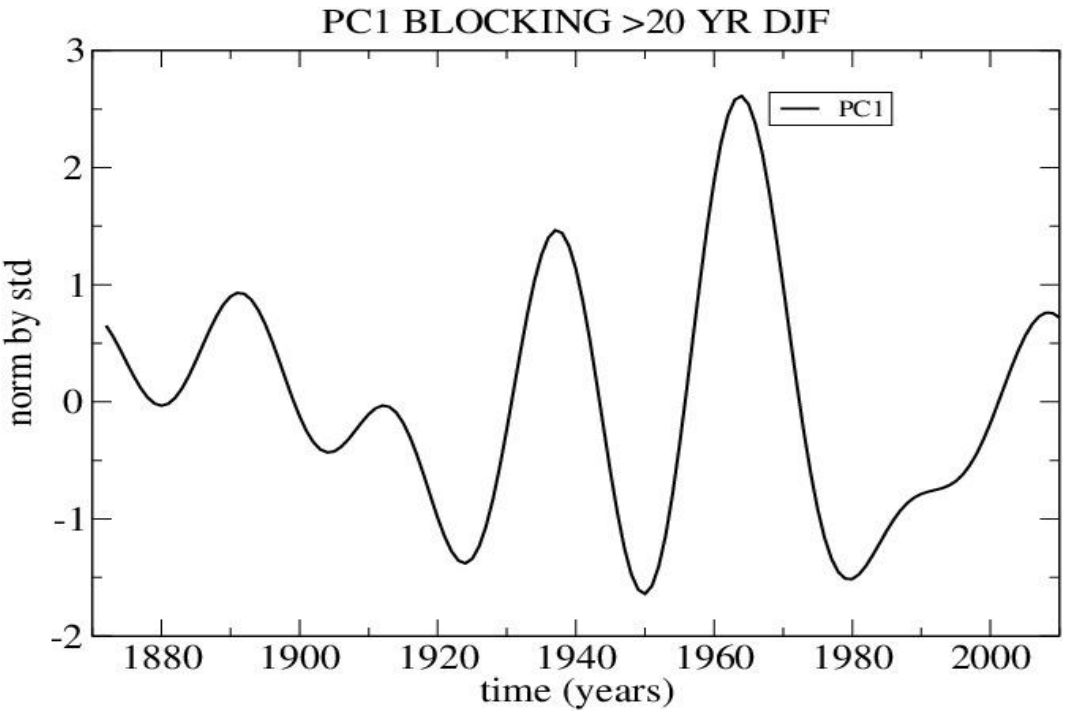
PC1 BLOCKING >20 YR DJF
PC1
norm by std
3
2
1
0
-1
-2
1880
1900
1920
1940
1960
1980
2000
time (years)

a)

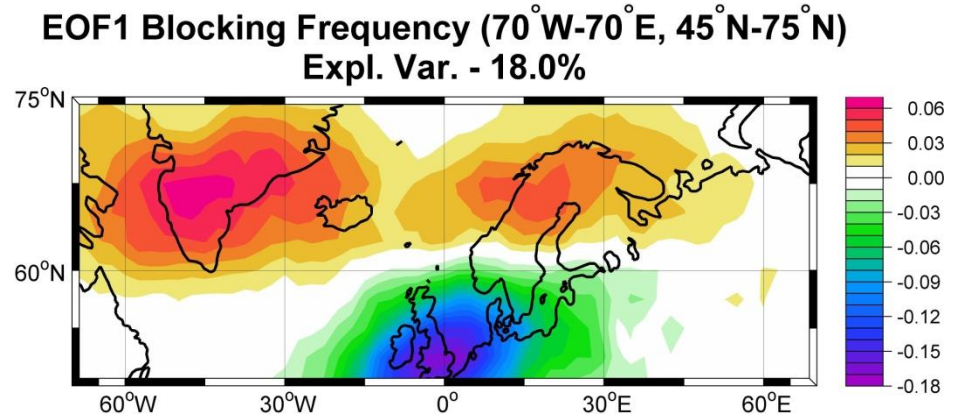
EOF1 Blocking Frequency (70°W-70°E, 45°N-75°N)
Expl. Var. - 18.0%
75°N
60°N
60°W
30°W
0°
30°E
60°E
0.06
0.03
0.00
-0.03
-0.06
-0.09
-0.12
-0.15
-0.18

b)

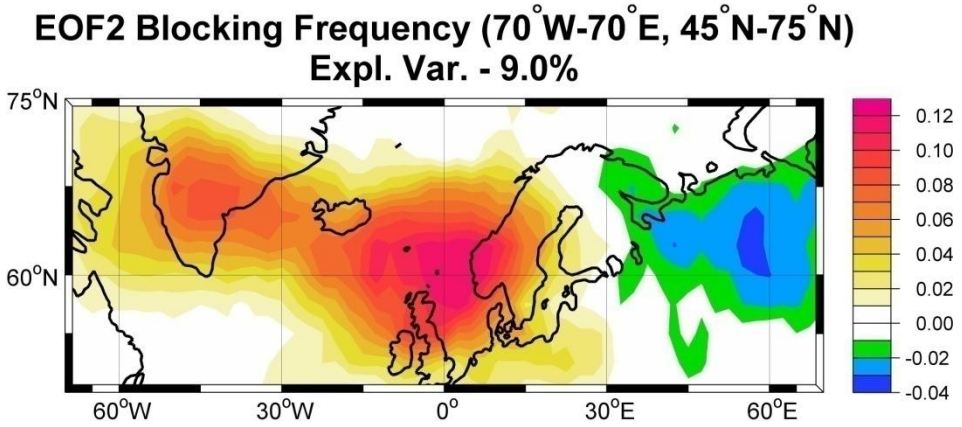
EOF2 Blocking Frequency (70°W-70°E, 45°N-75°N)
Expl. Var. - 9.0%
75°N
60°N
60°W
30°W
0°
30°E
60°E
0.12
0.10
0.08
0.06
0.04
0.02
0.00
-0.02
-0.04

c)

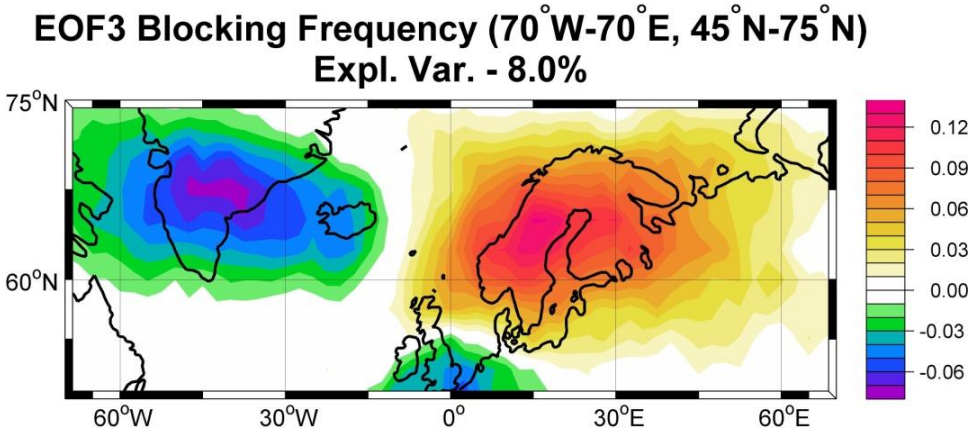
EOF3 Blocking Frequency (70°W-70°E, 45°N-75°N)
Expl. Var. - 8.0%
75°N
60°N
60°W
30°W
0°
30°E
60°E
0.12
0.09
0.06
0.03
0.00
-0.03
-0.06